IAEA
International Atomic Energy Agency

XRF techniques for materials and life sciences

Alessandro Migliori

Nuclear Science and Instrumentation Laboratory

International Atomic Energy Agency

Annual Training Workshop on Synchrotron Technologies and Techniques and their Applications, Elettra Sincrotrone Trieste, 26-30 May 2025

❑ Conventional XRF

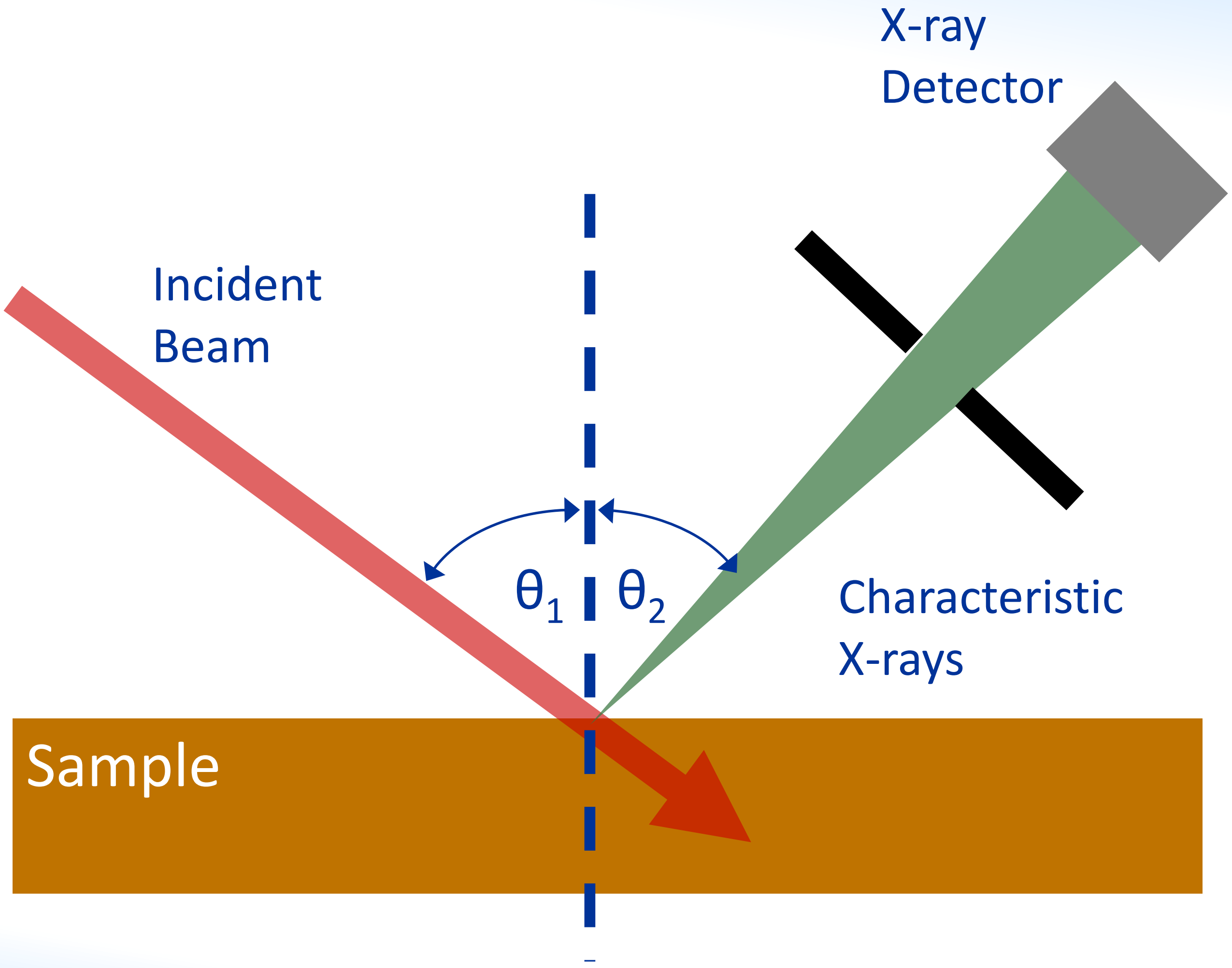

Sources of ionizing radiation

- Electrons (SEM)
- Charged particles (accelerators)
- Radioisotopes (α, **γ**, **X-rays**)
- **X-ray Tubes**
- **Synchrotron radiation**

❑ Interaction of X-rays with matter

X-rays can interact with the atoms of the material in two different ways:

- **Photoelectric effect**: Primary X-ray radiation can ionise atoms of the material. The X-ray is absorbed in this process

- **Scattering**:
  - ✓ **Elastic/Coherent scattering** (**Rayleigh**): no energy loss after collision with electrons. The Rayleigh effect is present when electrons are strongly bound (inner atomic electrons)
  - ✓ **Inelastic/Incoherent scattering** (**Compton**): energy loss after collision with electrons. The Compton effect is present when electrons are loosely bound (outer, less bound electrons)

❑ Photoelectric effect

Photoelectric effect: Primary X-ray radiation can ionise atoms of the material to be analysed

Cross section of the PE depends strongly on *Z* of the material and on the energy of the primary X-ray

$$\sigma_{Ph} \propto \frac{Z^n}{E_X^{3.5}} \qquad n = 3 \div 4$$

To maximize the ionization probability, the energy of the primary X-ray should be higher than the binding energy but as close as possible to it

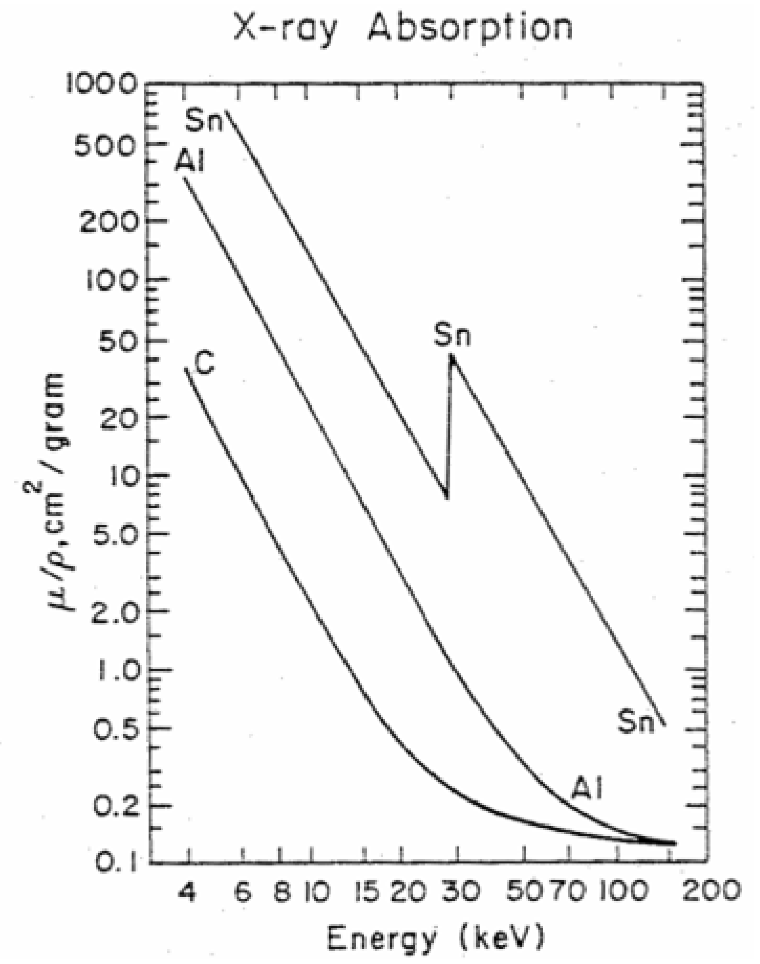

❑ X-Ray Fluorescence

Incident photon Energy E_0 should be adequate to ionize the atomic bound electrons **→ $E_0 \geq$ inner shell binding energy**

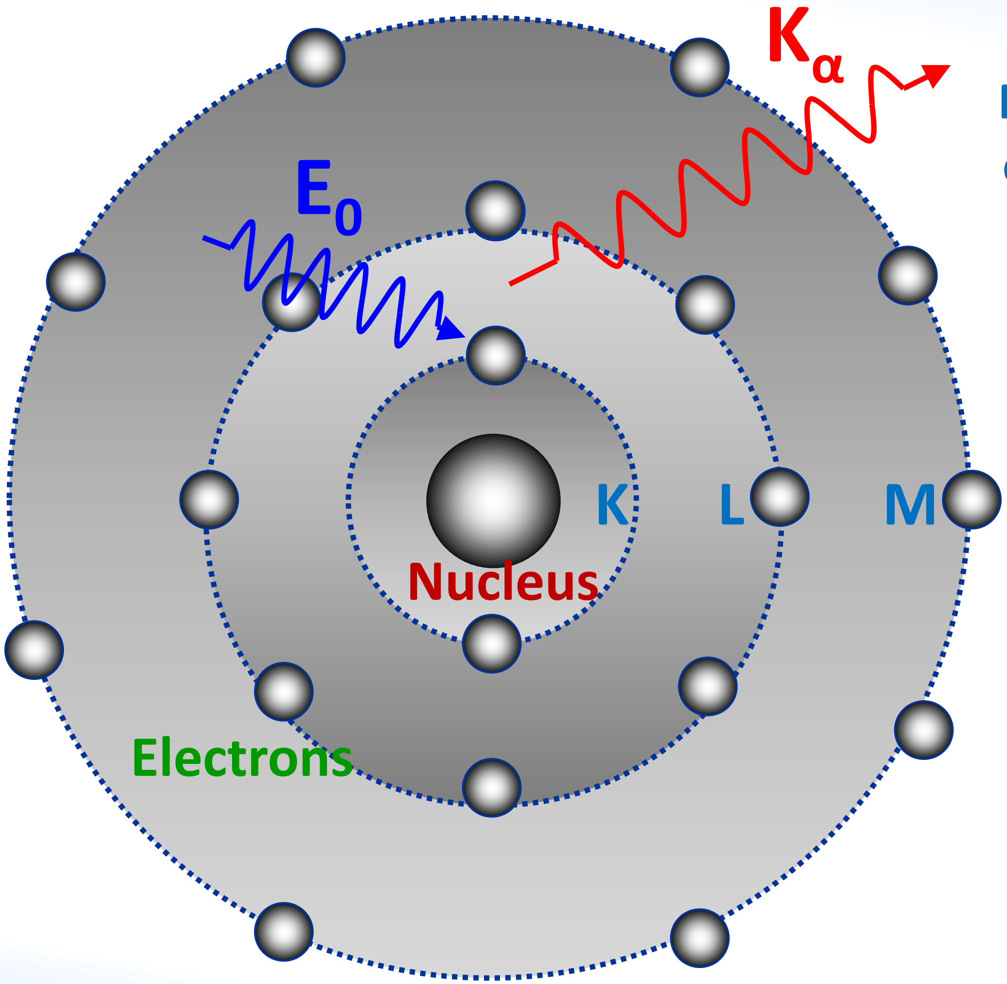

Photo-Ionization of atomic bound electrons (K, L, M) (**Photoelectric absorption**)

Electronic transition and emission of element **→ characteristic fluorescence** radiation

Fluorescence X-ray emission is **isotropic**

❑ De-excitation: Fluorescence/Auger

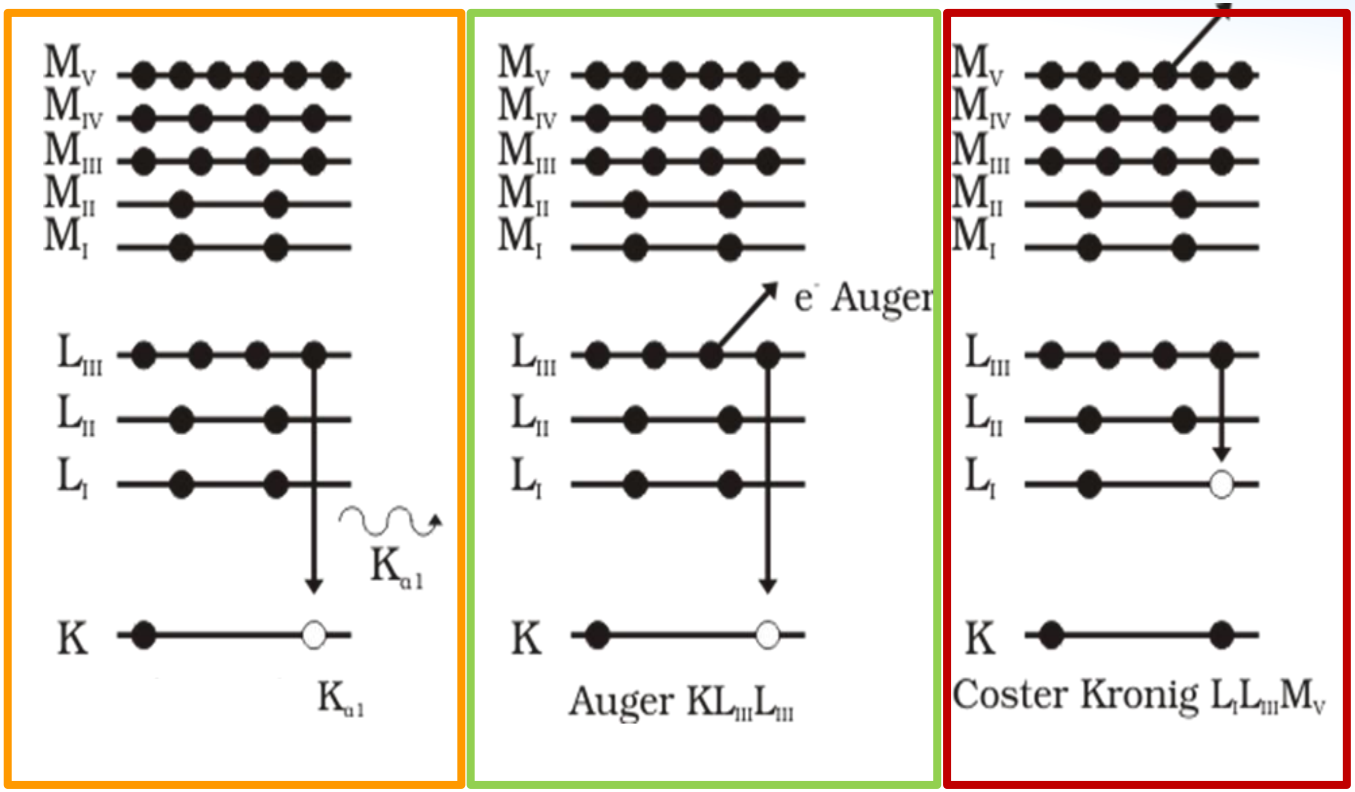

Emission of characteristic X-ray

Emission of electron (vacancy filled by electron from different shell)

Emission of electron (vacancy filled by electron from the same shell)

Fluorescence yield

The fluorescence yield is given by the **ratio of the emitted fluorescence photons over the number of the created holes**. The competing process is the **emission of Auger electrons** as the atom returns to its ground state

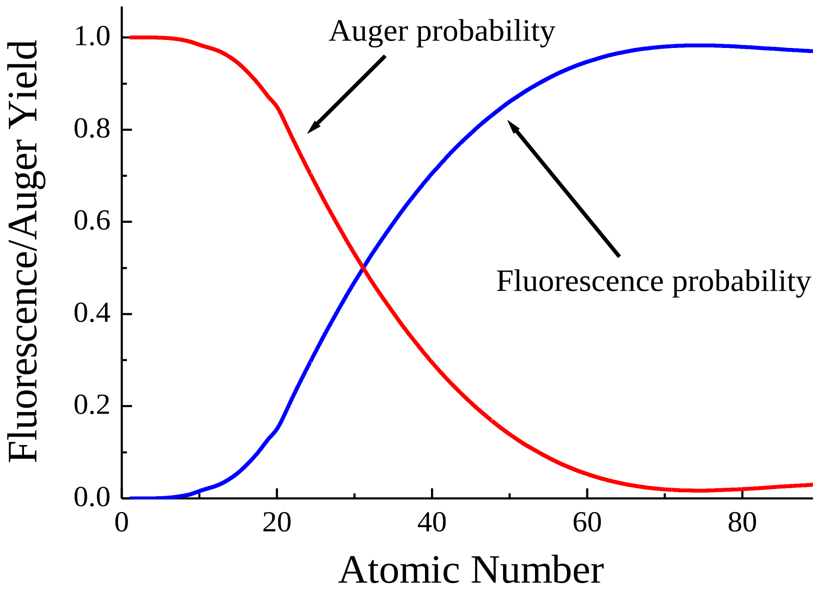

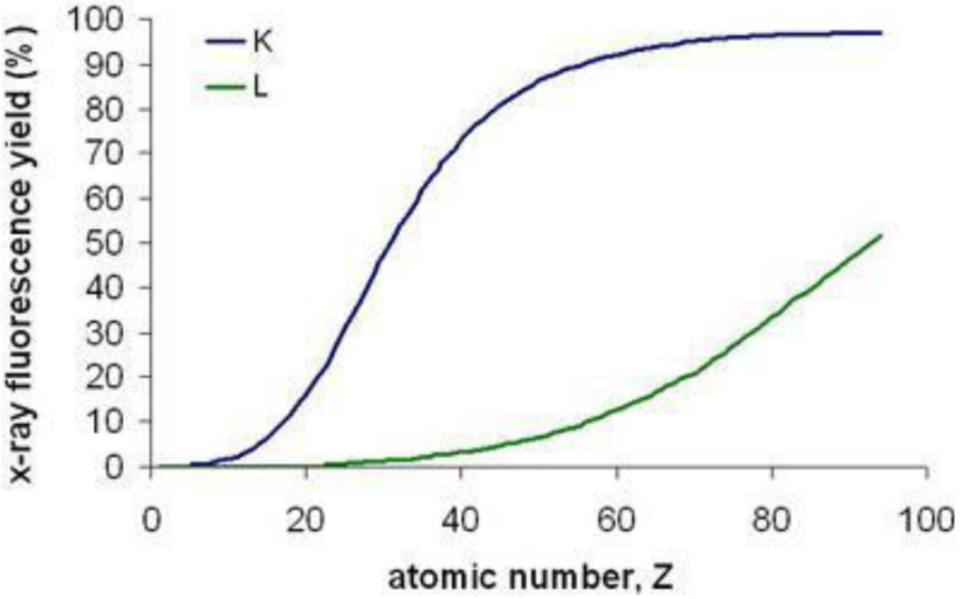

For low Z the Auger electron emission is dominant

❑ Emission of characteristic X-rays

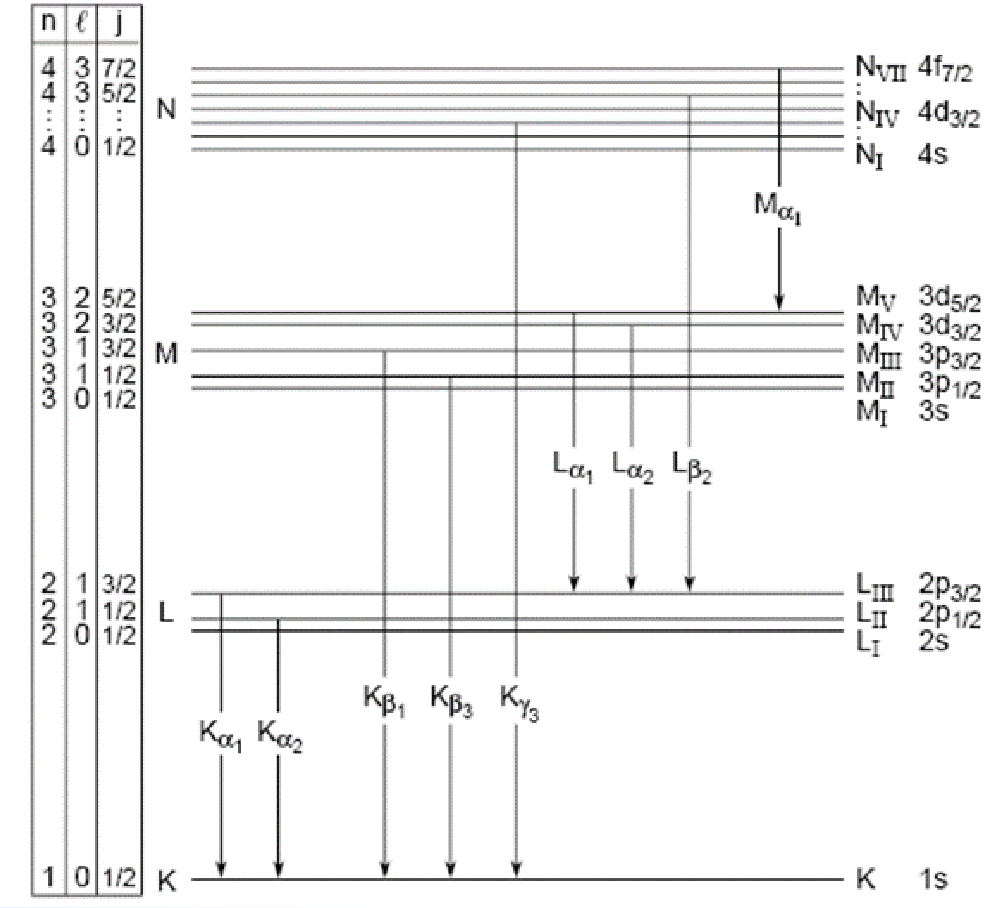

The emission of characteristic X-ray lines follows allowed electronic transitions between specific subshells

Each element has a unique set of emission lines

Siegbahn/IUPAC notation:

K_α: K-L_2 + K-L_3

K_β: K-M_2 + K-M_3

L_α: L_3-M_4 + L_3-M_5

$L_{\beta 1}$: L_2-M_4

$L_{\beta 2}$: L_3-N_5

❑ X-ray energies

Moseley's law

$$E = h \cdot A \cdot R \cdot (Z - b)^2$$

h = Planck constant
R = Rydberg frequency
Z = atomic number
A = 3/4 for K_{α}, 5/36 for L_{α}
b = 1 for K_{α}, 7.4 for L_{α}

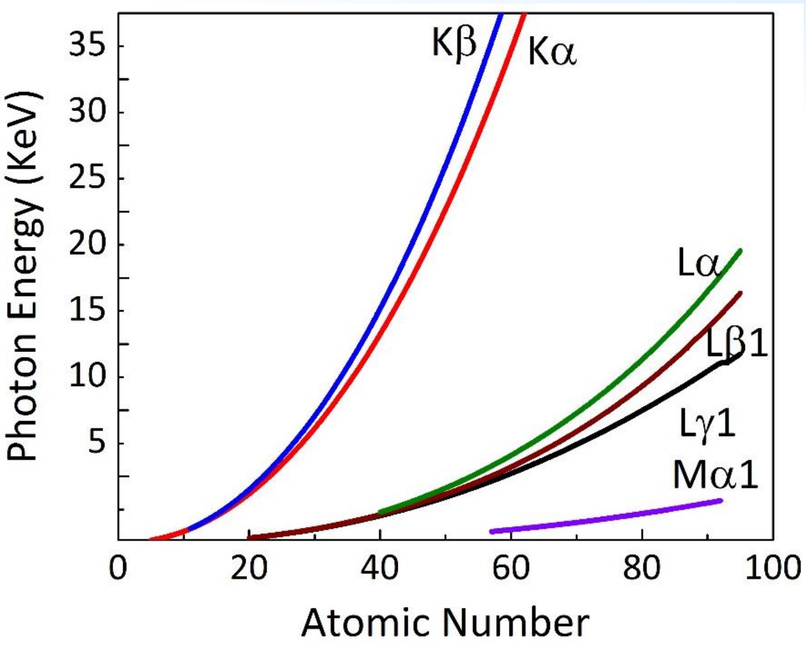

K_{α}	$E\,[\text{eV}] \approx 10.20 \cdot (Z - 1)^2$	$E_{Fe\text{-}K\alpha} \approx 6380$ eV
L_{α}	$E\,[\text{eV}] \approx 1.89 \cdot (Z - 7.4)^2$	$E_{Pb\text{-}L\alpha} \approx 10520$ eV

X-ray spectroscopy within the energy range 1÷30 keV offers in principle the possibility to detect all the periodic table elements ($Z > 10$) through their K, L or even M series of emission lines

❑ X-ray scattering

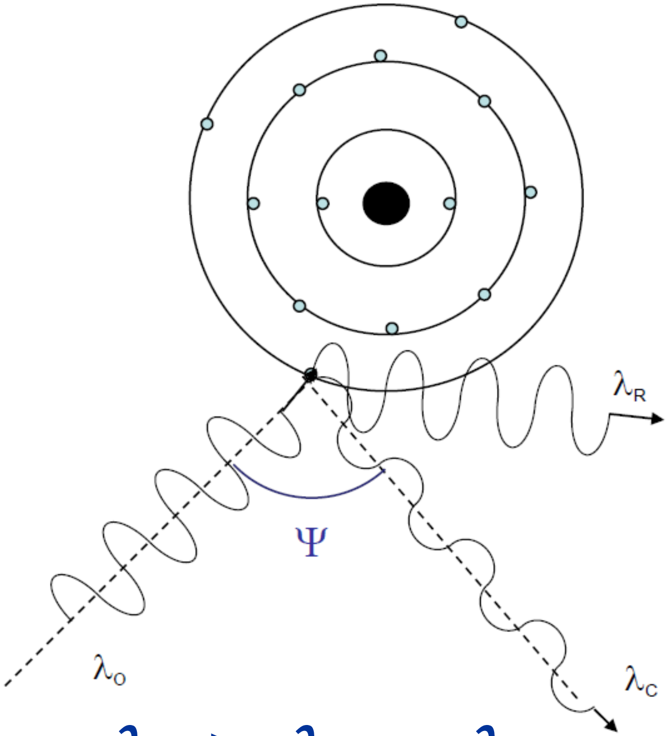

$$\lambda_C > \lambda_R = \lambda_0$$

Elastic/coherent scattering (Rayleigh):
no energy loss after collision with electrons. The Rayleigh effect is present when electrons are strongly bound.
Rayleigh is more intense for high *Z* (= heavy) matrices

Inelastic/Incoherent scattering (Compton):
energy loss after collision with electrons. The Compton effect is present when electrons are loosely bound.
Compton is more intense for low *Z* (= light) matrices

❑ Rayleigh scattering

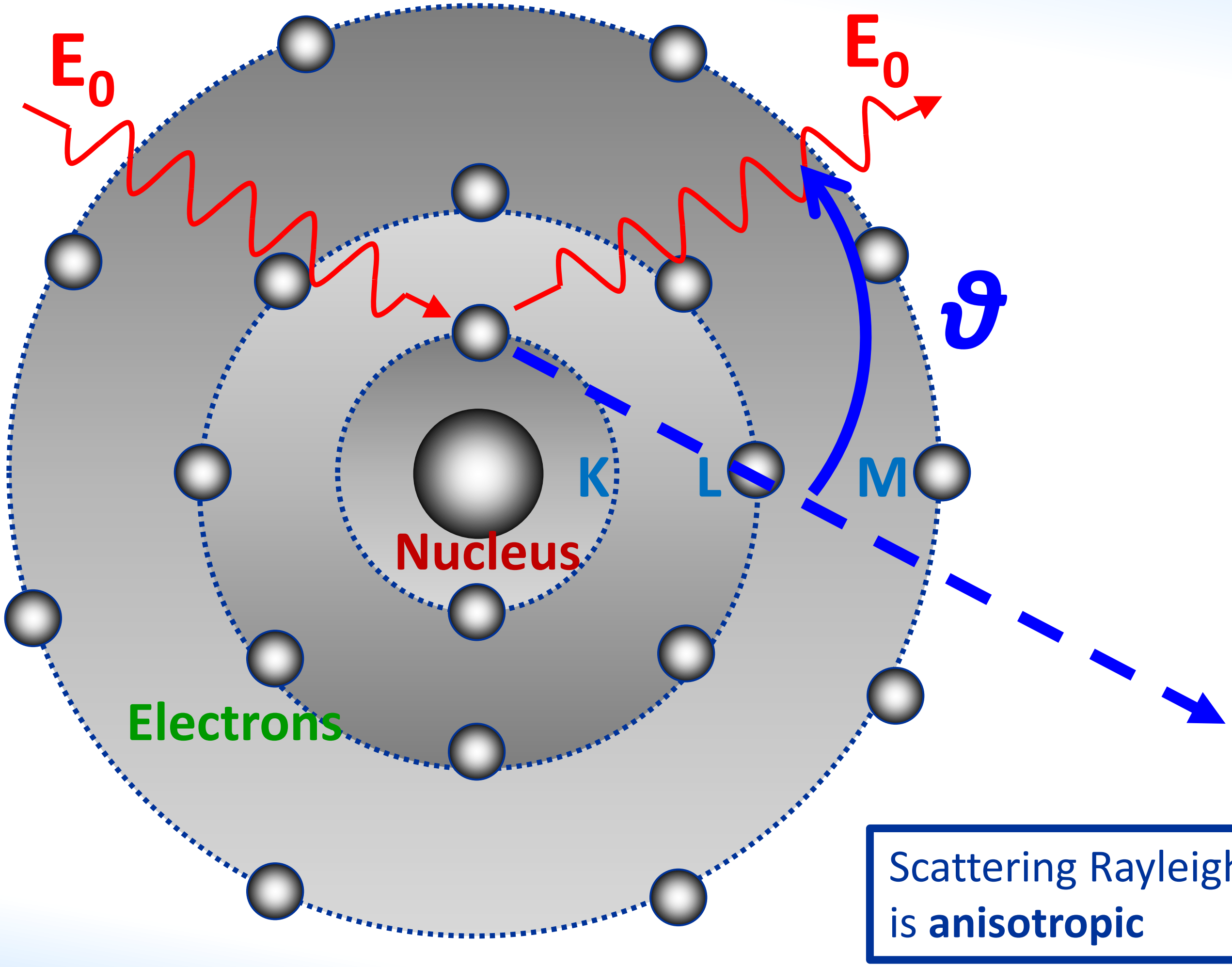

Incident photon Energy E_0

$E_i = E_0$: Coherent (Rayleigh)
It occurs mostly with inner atomic electrons

Scattering Rayleigh is **anisotropic**

❑ Compton scattering

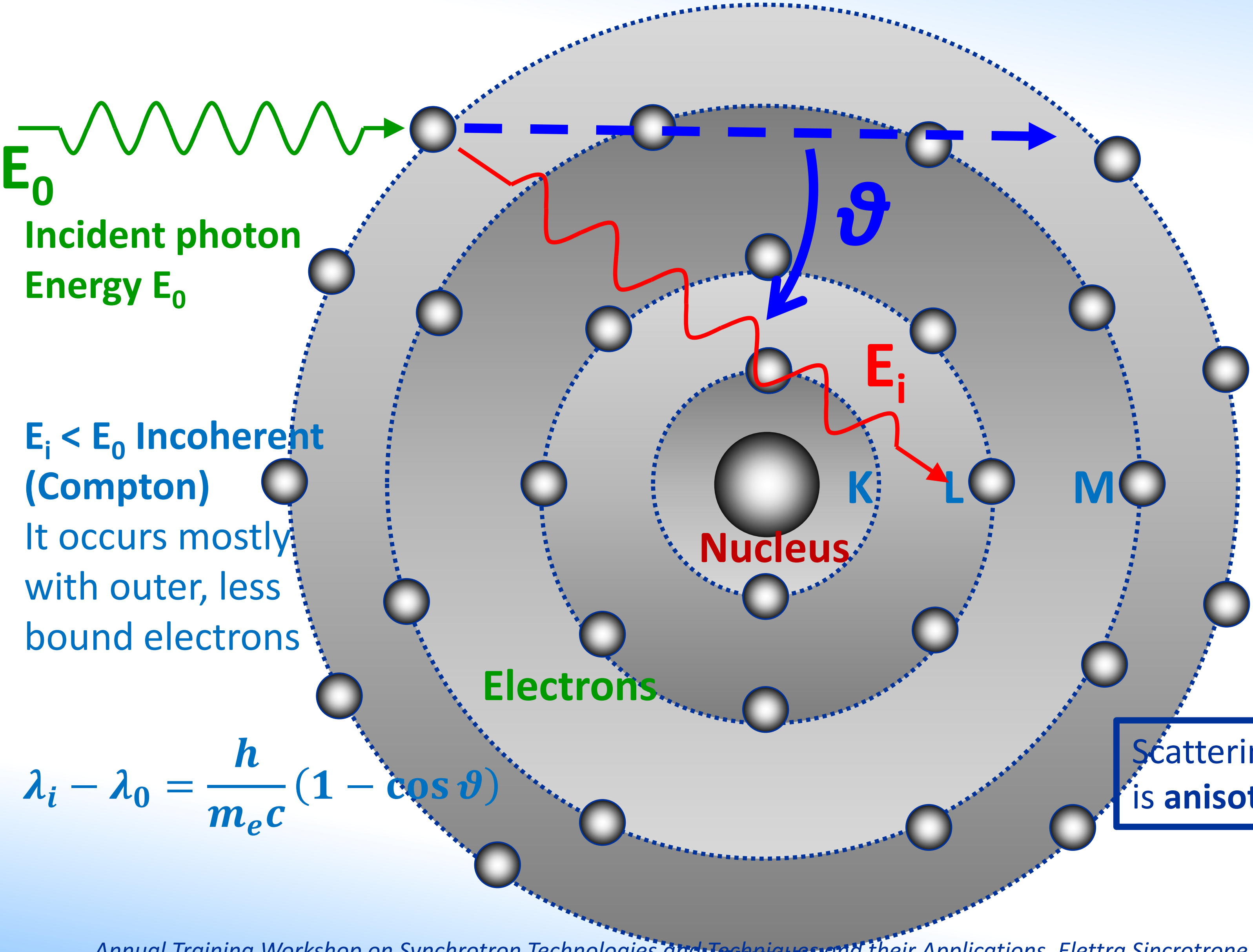

Incident photon
Energy E_0

$E_i < E_0$ Incoherent (Compton)

It occurs mostly with outer, less bound electrons

$$\lambda_i - \lambda_0 = \frac{h}{m_e c}(1 - \cos\vartheta)$$

Scattering Compton is **anisotropic**

❑ Linear attenuation coefficient *μ*

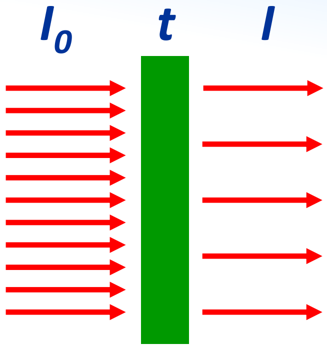

Attenuation of photons by a thin layer of thickness *dt* is described by

$$dI = I \cdot \mu \cdot dt$$

where *I* is the number of photons per unit area and unit time (photon flux) of which *dI* are attenuated while penetrating the layer of a material characterized by the (**total, linear**) **attenuation coefficient *μ***. This is equivalent to

$$I = I_0 \cdot e^{-\mu \cdot t}$$

I and I_0 are the photon fluxes behind and in front of the absorber, respectively, and *t* is the thickness. *μ* is a function not only of the material (atomic number *Z*) but also of the photon energy *E*

❑ Mass attenuation coefficient μ_m

$$\mu = \mu_m \cdot \rho$$

the total mass attenuation coefficient μ_m doesn't depend on the density ρ of the material.

The coefficient μ_m summarizes all possible photon interactions

$$\mu_m = \tau_m + \sigma_m$$

where τ_m describes the photo absorption and $\sigma_m = \sigma_{coh} + \sigma_{inc}$ are the contributions by coherent and incoherent scattering, respectively.

Both kinds of scattering contribute much less than the photo absorption to the total μ_m

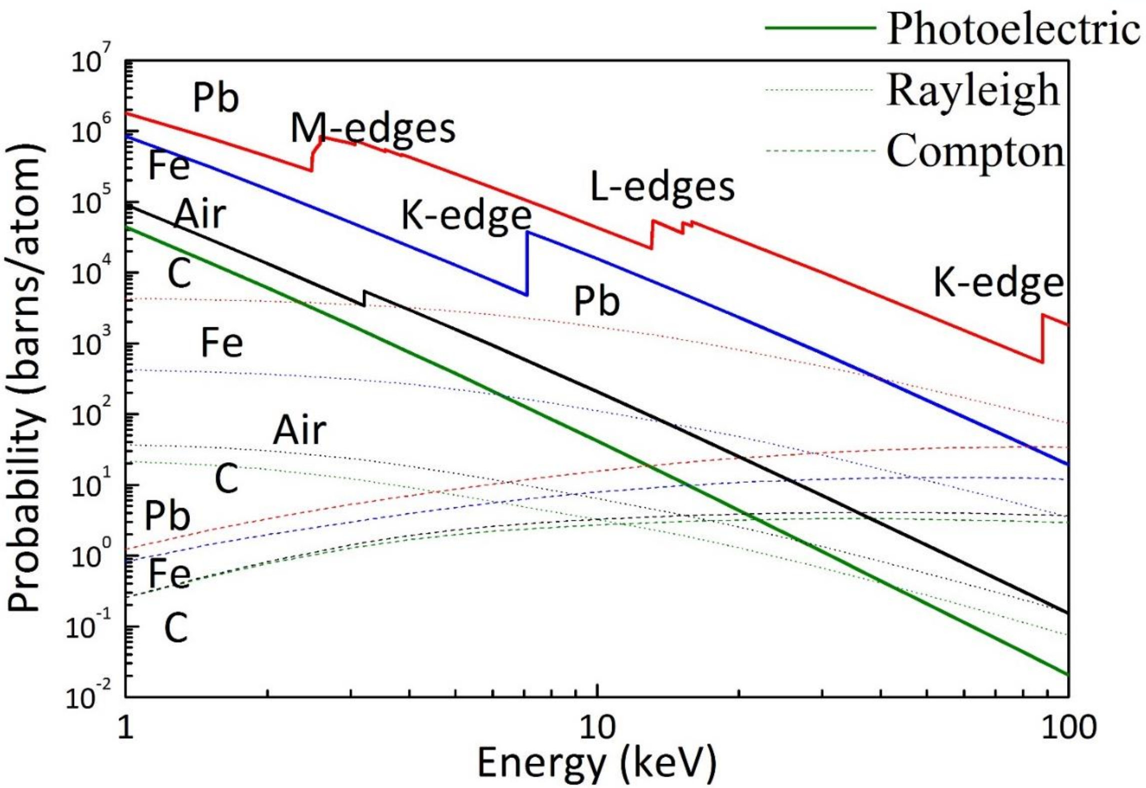

❑ Mass attenuation coefficient μ_m

the mass attenuation coefficient of a material that is composed of several elements, with weight fractions w_i , is

$$\mu_m = \sum_i w_i \cdot \mu_m^i$$

Use of mass attenuation coefficients suggests replacing the thickness by the **area-related mass** $m = M/A$ (mass M per unit area A) and rewriting the attenuation law as

$$I = I_0 \cdot e^{-\mu_m \cdot m}$$

$t \cdot \rho = M/A$, in **grams/cm²**

❑ Penetration and information depth

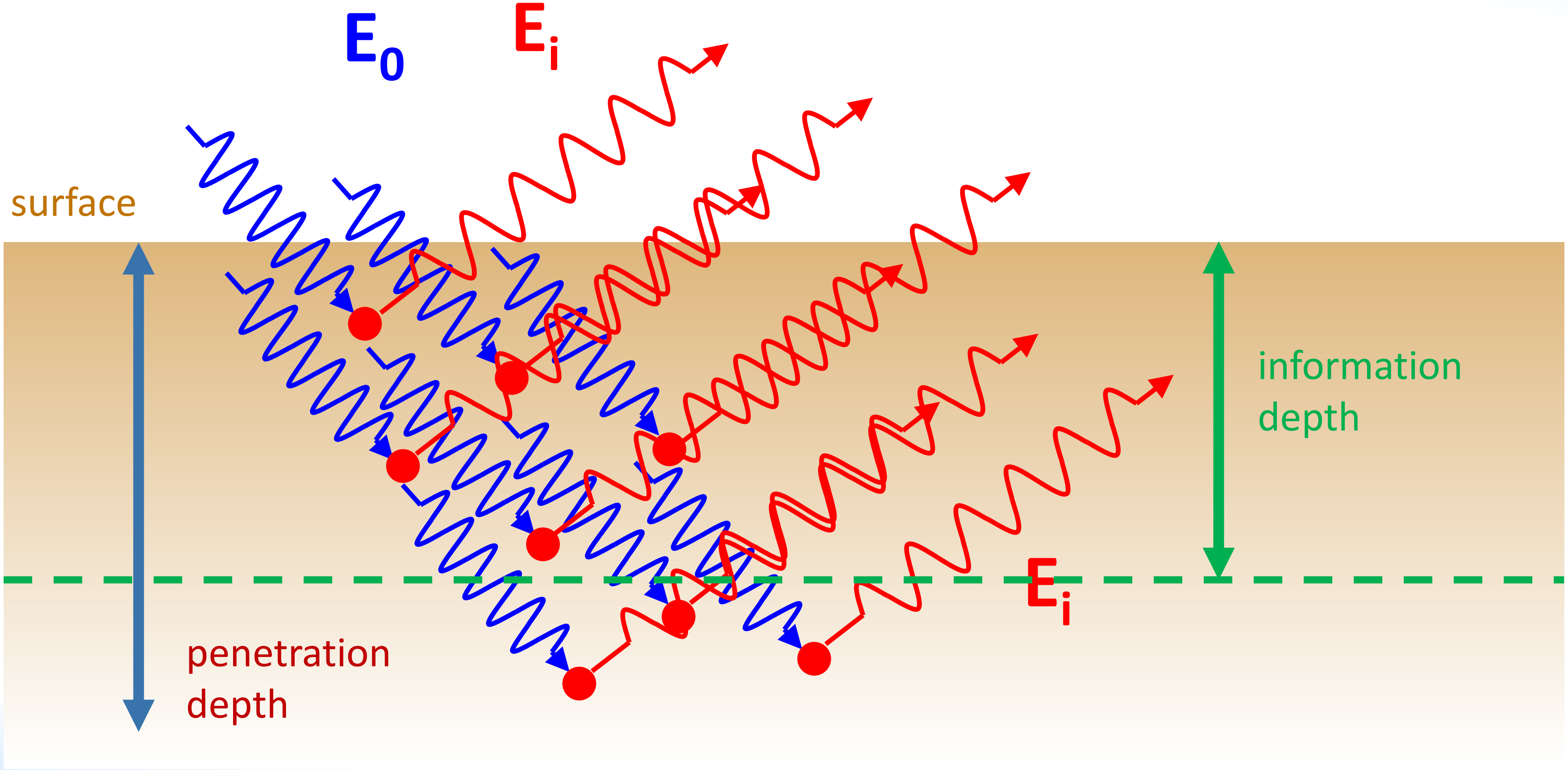

Penetration and information depth

Penetration and information (analytical) depth depend on the energy of the X-ray and on the matrix:

surface

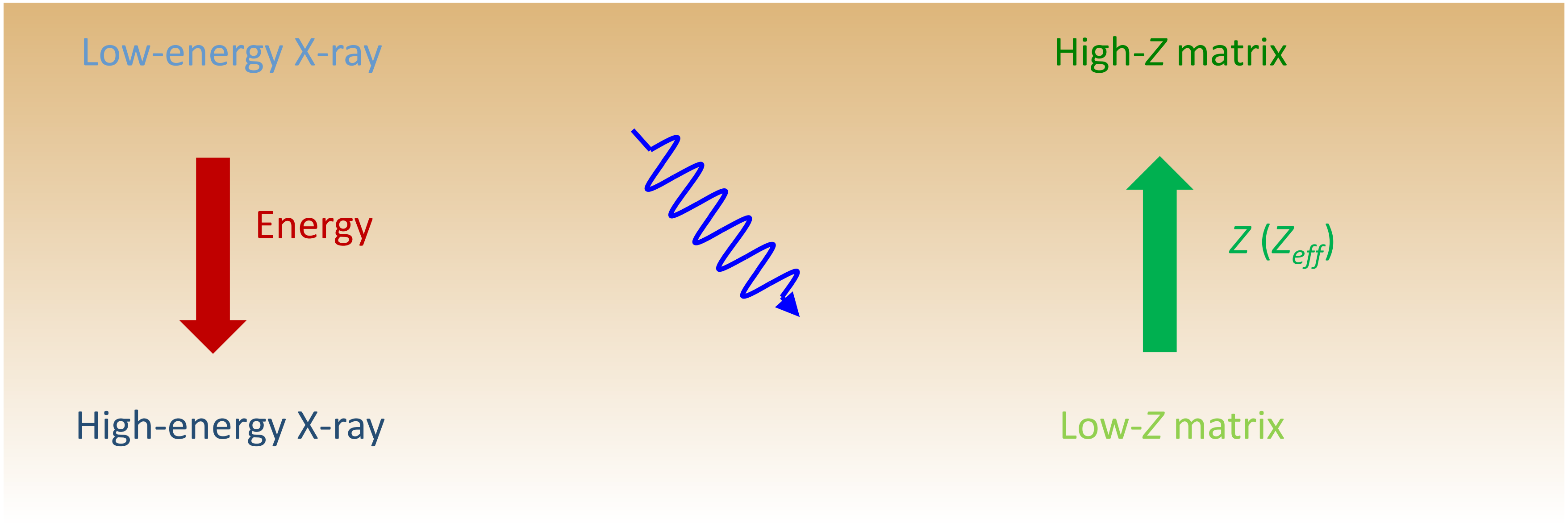

Low-energy X-ray

High-Z matrix

Energy

Z (Z_{eff})

High-energy X-ray

Low-Z matrix

- **Surface treatment is extremely important for heavy matrices**
- **Information thickness is essential for light matrices**

❑ Influence of sample thickness

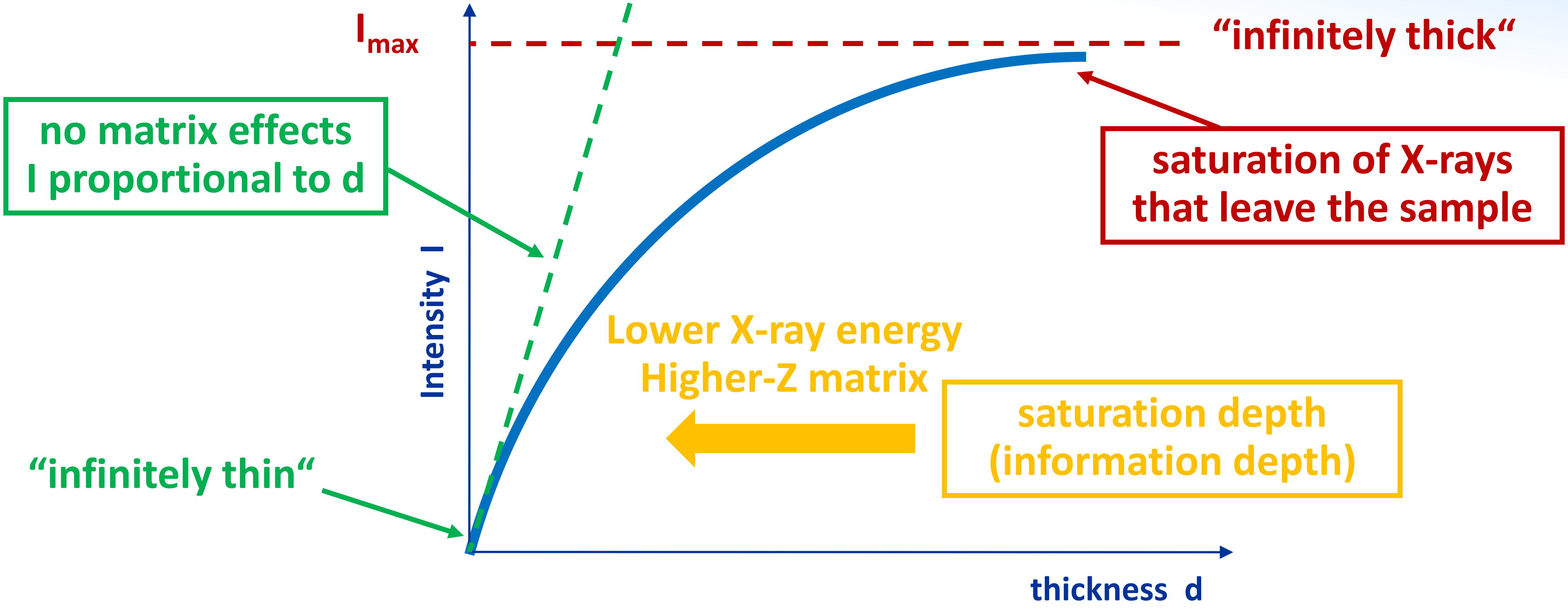

“infinitely thick“

no matrix effects
I proportional to d

saturation of X-rays
that leave the sample

Lower X-ray energy
Higher-Z matrix

saturation depth
(information depth)

“infinitely thin“

Increasing the thickness of the sample above the information depth will not increase the signal but only the scattering of the primary radiation

❑ Analytical depths in different matrices

Different elements exhibit different Information thicknesses (99%), depending on their characteristic X-ray energy and on the overall matrix

Line	Energy	Graphite	Glass	Iron	Lead
Cd $K_{\alpha 1}$	23,17 keV	14,46 cm	8,20 mm	0,70 mm	77,30 µm
Mo $K_{\alpha 1}$	17,48	6,06	3,60	0,31	36,70
Cu $K_{\alpha 1}$	8,05	5,51 mm	0,38	36,40 µm	20,00
Ni $K_{\alpha 1}$	7,48	4,39	0,31	29,80	16,60
Fe $K_{\alpha 1}$	6,40	2,72	0,20	*164,00	11,10
Cr $K_{\alpha 1}$	5,41	1,62	0,12	104,00	7,23
S $K_{\alpha 1}$	2,31	116,00 µm	14,80 µm	10,10	4,83
Mg $K_{\alpha 1}$	1,25	20,00	7,08	1,92	1,13
F $K_{\alpha 1}$	0,68	3,70	1,71	0,36	0,26
N $K_{\alpha 1}$	0,39	0,83	1,11	0,08	0,07
C $K_{\alpha 1}$	0,28	*13,60	0,42	0,03	0,03
B $K_{\alpha 1}$	0,18	4,19	0,13	0,01	0,01

E_{KC} = 0.2842

E_{KFe} = 7.112

❑ Detectors

- Proportional Counters
- Scintillation Detectors
- Si(Li)
- LEGe
- PIN Diode
- **SDD**
- CCD, CMOS cameras
- CZT, other

❑ Semiconductor detectors

- X-rays produce **electron-hole pairs**, whose number is **proportional** to the energy of the radiation (average energy to produce an electron/hole pair is 3.6eV for Si and 2.9eV for Ge)
- Electrons and holes are collected from the depleted active region to the electrodes, where they result in a **pulse** that can be further **amplified** and finally **measured**
- This pulse carries information about the energy of the original incident radiation. The number of such pulses per unit time also gives information about the intensity of the radiation

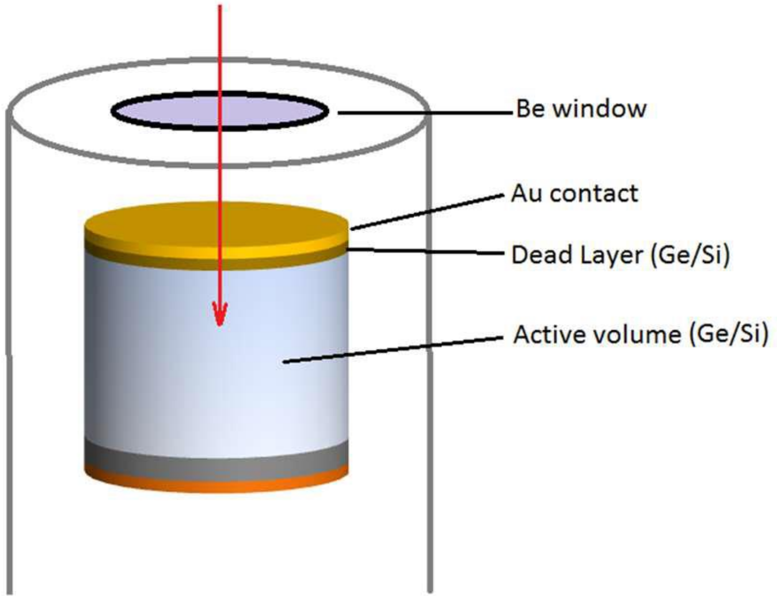

❑ Silicon Drift Detectors - SDD

The charge is drifted from a large area into a small read-out node with low capacitance, independent of the active area of the sensor. Thus, the serial noise decreases, and shorter shaping time can be used. For SDDs faster counting is enabled and higher leakage current can be accepted, drastically reducing the need for cooling.

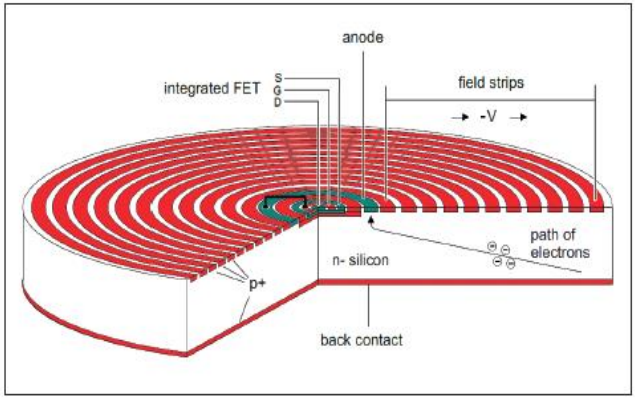

- Energy resolution ~ 125 – 140 eV (Mn-Ka)
- Input capability ~ 10^6 photons/sec

https://tools.thermofisher.com/content/sfs/brochures/TN52342_E_0512M_SiliconDrift_H.pdf

Detector photograph reproduced from https://www.rayspec.co.uk/x-ray-detectors/silicon-drift-detectors/xrf/

❑ Efficiencies of different detectors

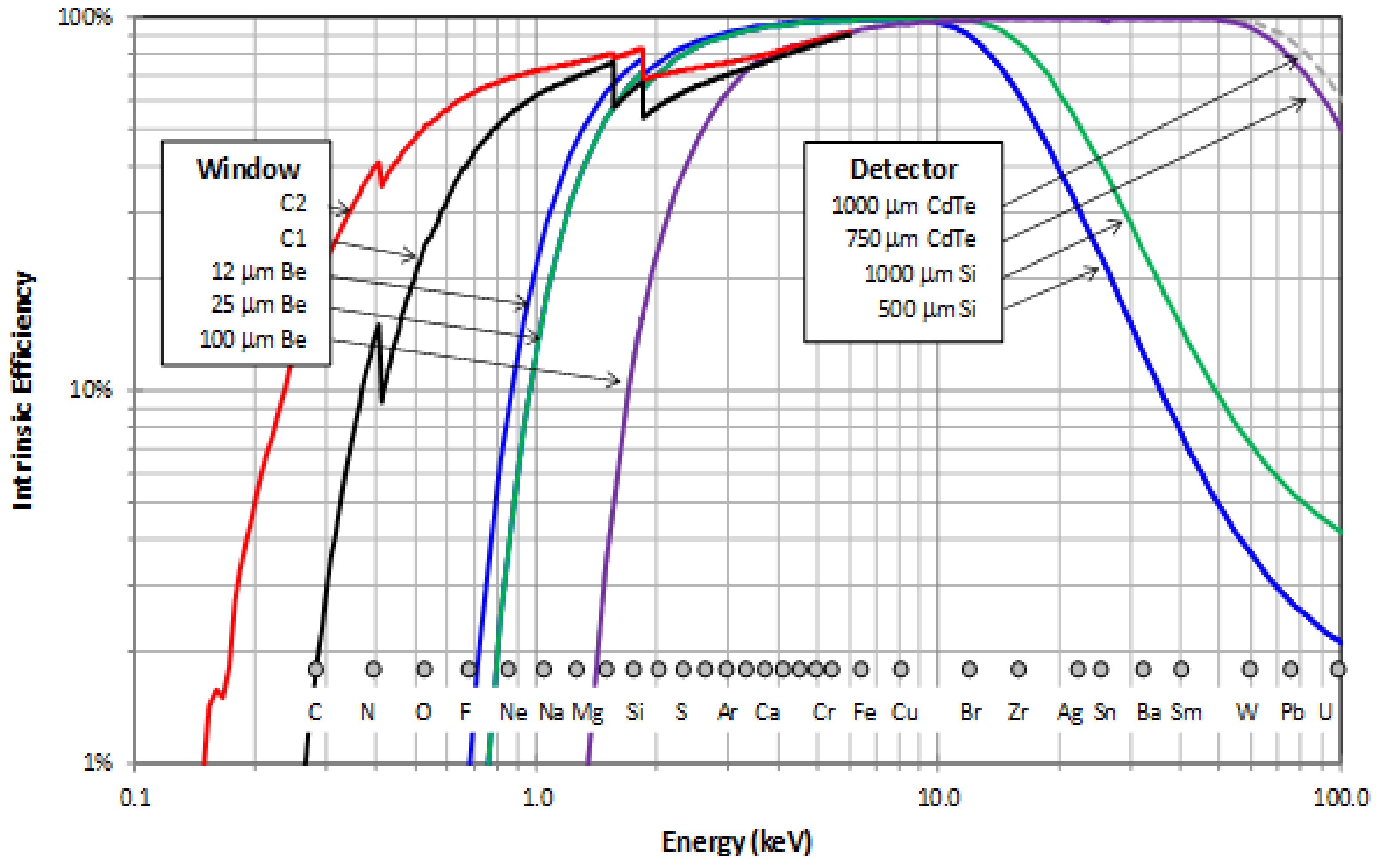

Comparison of different detector’s efficiency from AMPTEK
https://www.amptek.com/products/x-ray-detectors/fastsdd-x-ray-detectorsfor-xrf-eds/fastsdd-silicon-drift-detector

❑ “Light” elements (Na, Mg, Al, Si)

Vacuum atmosphere or **He flushing** is required in the x-rays path between sample and detector

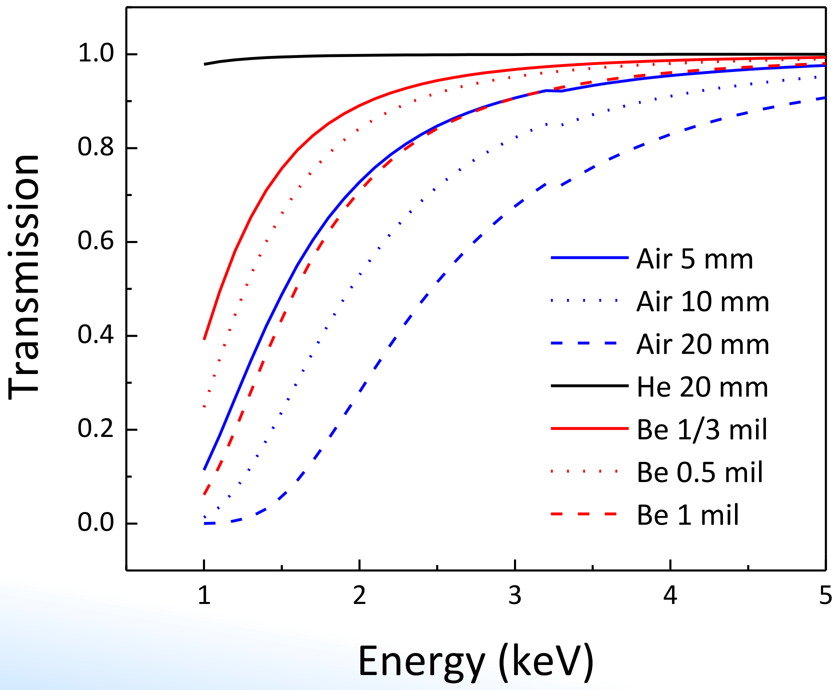

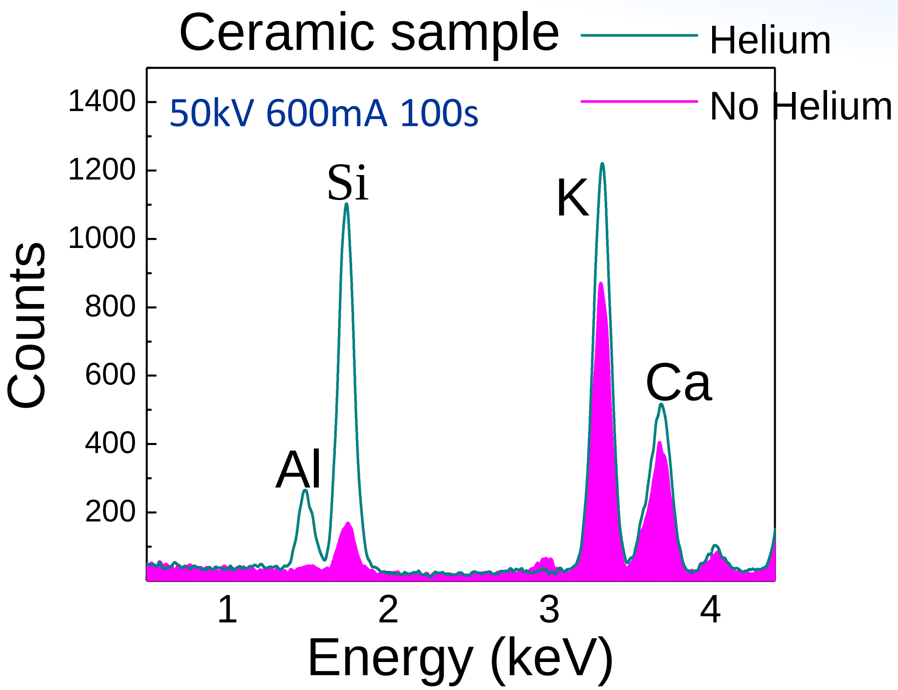

The improvement in the intensity of Al-K and Si-K characteristic X-ray lines is significant, 22 and 7.3 times respectively

❑ Typical EDXRF spectrum

- Escape peaks (Ca-Ka – 1.74 keV = 1.95 keV)

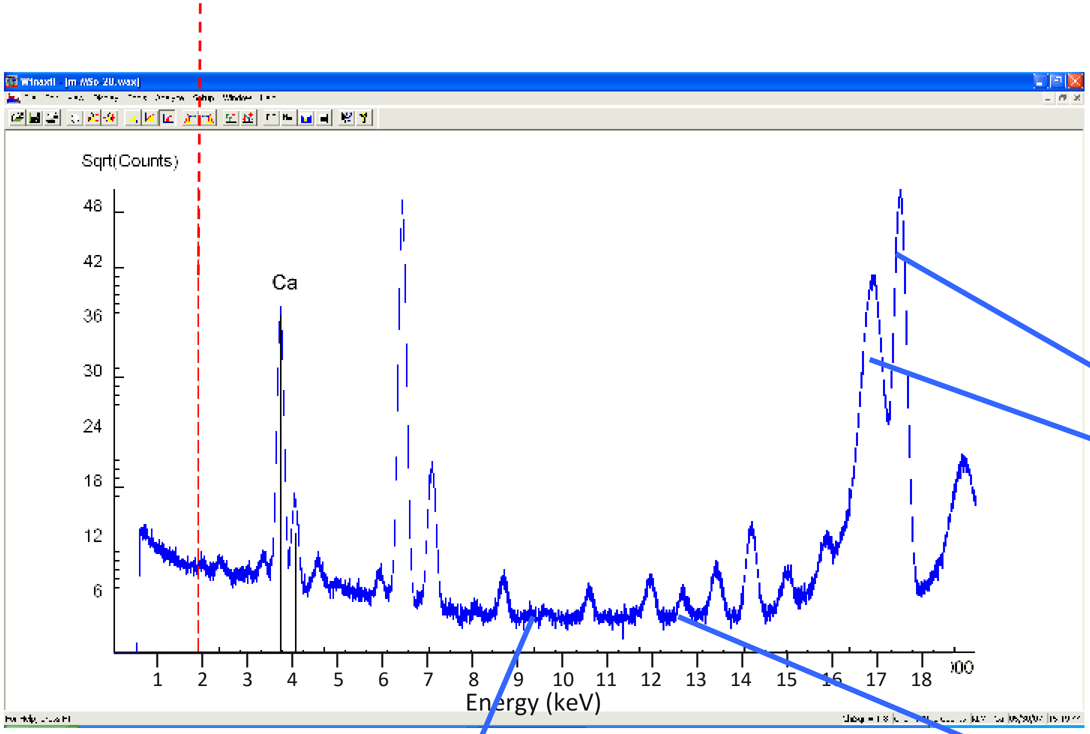

- Characteristic radiation
  - ✓K, L or M-lines
- Scatter
  - ✓Coherent
  - ✓Incoherent
- Sum peaks

  Fe-Ka + Fe-Ka= 12.8 keV

- Continuum radiation

❑ Resolution of EDXRF spectrometers

Full Width at Half Maximum (FWHM) of a peak

$$FWHM^2_{Peak} = FWHM^2_{Elec} + FWHM^2_{Det}$$

Electronic noise:
~100 eV

Intrinsic contribution:

$$2.3548\sqrt{\varepsilon \times F \times E}$$

ε Energy to create e-h pair (3.85 eV)

F Fano factor (~0.114)

E x-ray energy in eV

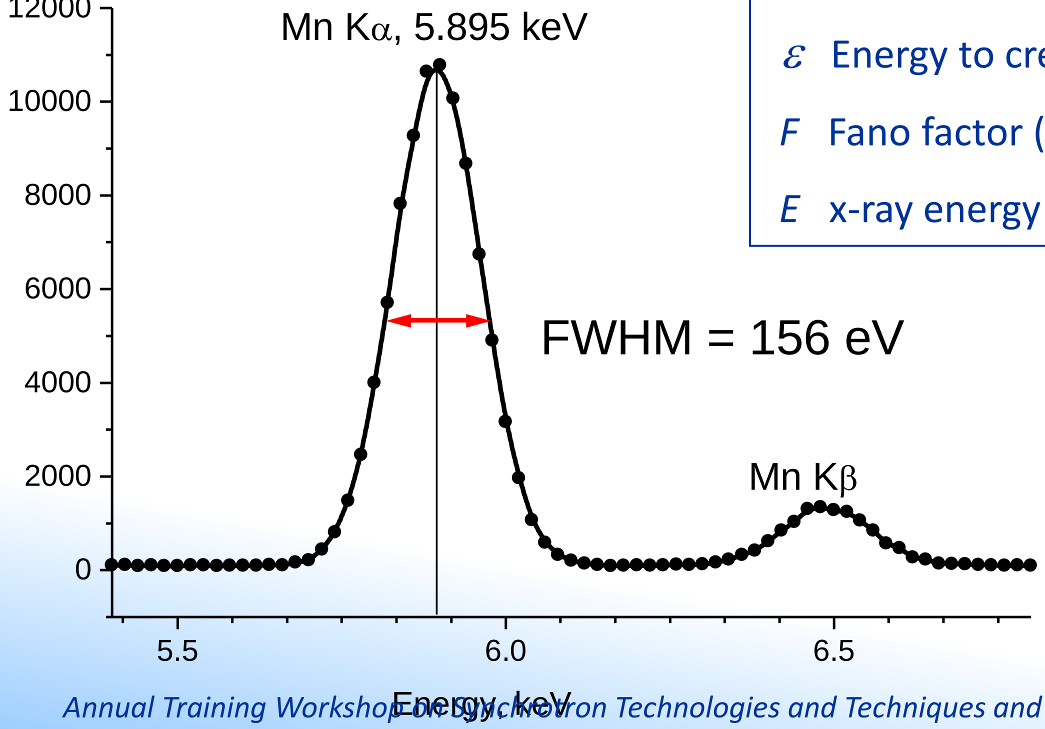

Mn Kα @ 5.895 keV

$FWHM_{Det}$ = 120 eV

$FWHM_{Elec}$ = 100 eV

=> $FWHM_{Peak}$ = 156 eV

❑ Cr-Mn-Fe overlap at ~160 eV

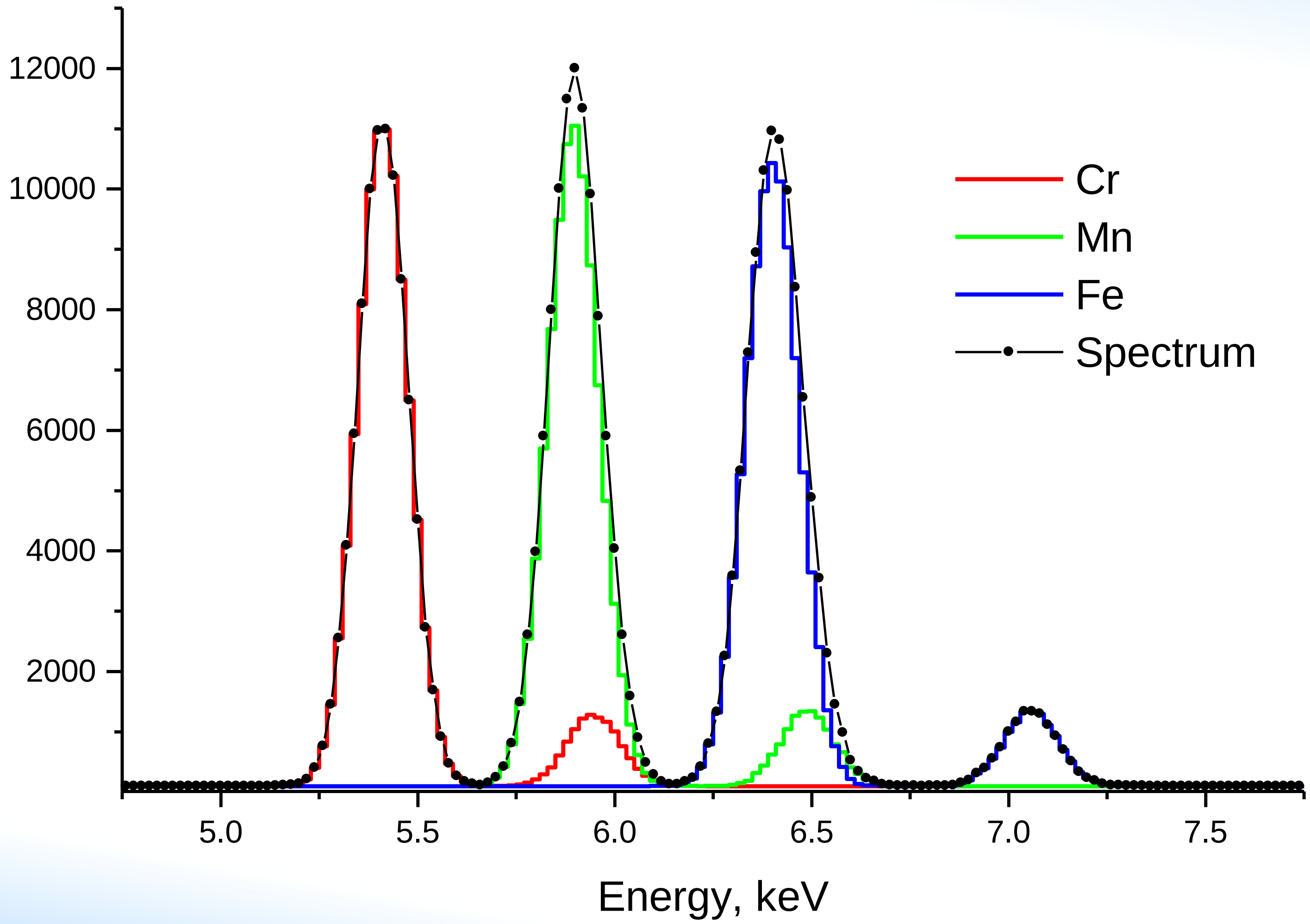

❑ Case of strong overlapping

Overlapping of As-Kα (about 10.54 keV) and Pb-Lα lines (about 10.55 keV)

Binding energies:

As-K = 11.87keV

Pb-L_3 = 13.04keV
Pb-L_2 = 15.20keV
Pb-L_1 = 15.86keV

Arsenic can be easily quantified at synchrotron using an energy
11.87 keV < E < 13.04 keV

❑ The Shermann-Nikina formulae

$$I_i = \varepsilon(E_i) w_i \int_{E>E_i^{ab}}^{E_{\max}} G K_i A(E_0, E_i) R_i(E_0, E_j) I_0(E_0) dE_0$$

$K_i = \frac{J_K^i - 1}{J_K^i} \omega_K^i f_{K_\alpha}^i \tau_i(E_0)$	Contains all the fundamental parameters for specific k-line of element *i*
$A_S(E_0, E_i) = \frac{1 - e^{-\chi_S (E_0, E_i) \rho x}}{\chi_S (E_0, E_i)}$	Takes into account the attenuation of both excitation and fluorescent radiation in the sample
$R_i(E_0, E_j)$	Considers the enhancement of x-ray production of element *i* by the characteristic of other major elements *j* present in the sample and having characteristic energies larger than absorption edge of element *i*
$I_0(E_0)$	Is the probability distribution by energies of the excitation radiation
$\varepsilon(E_i)$	Is the efficiency of the detector for energy E_i
G	Is the overall effective solid angle for excitation and detection

Spurious peaks in XRF spectra

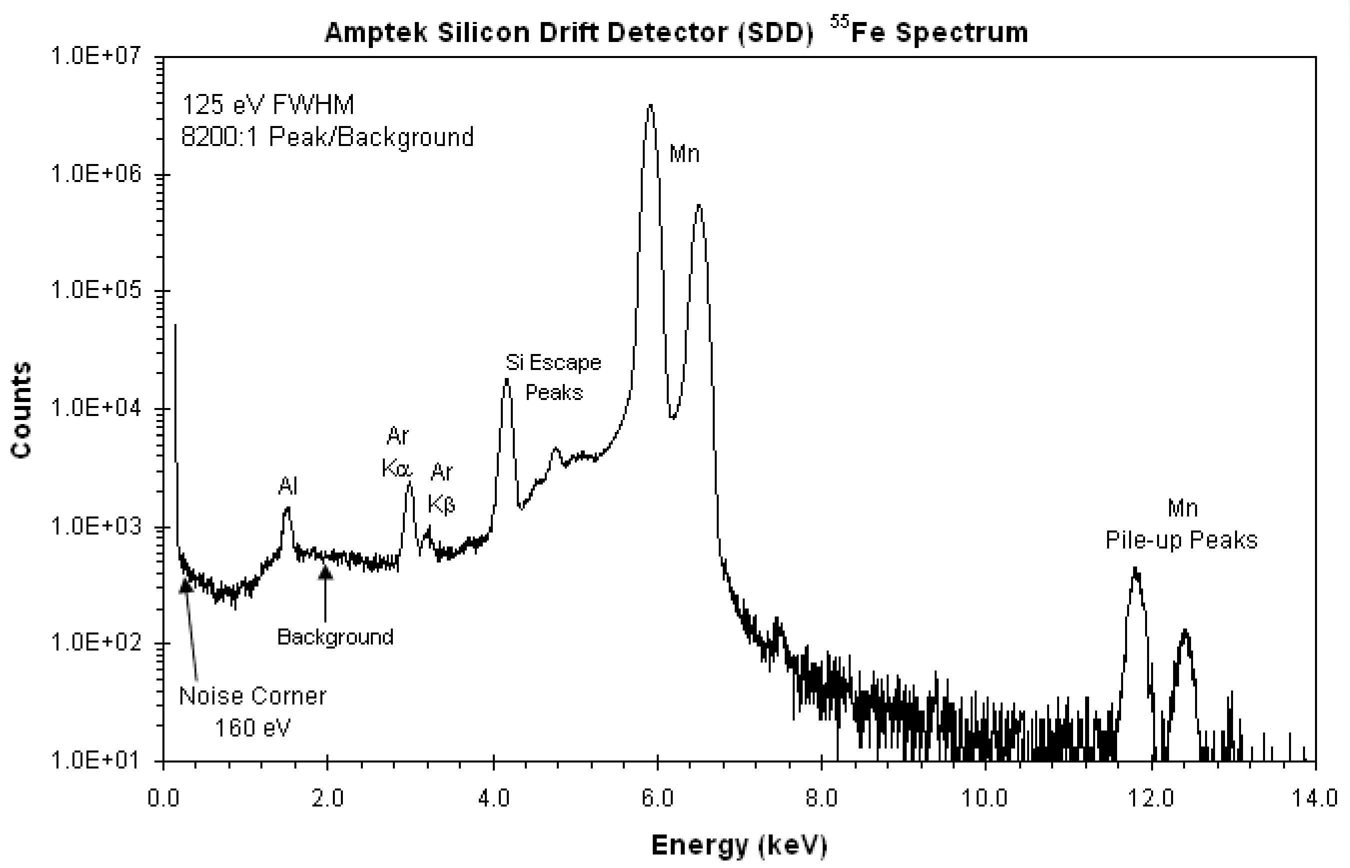

Spectrum from ^{55}Fe radioactive source

❑ Information obtained by XRF

Qualitative:

Which elements are present in the sample

Crucial for samples that are not homogeneous (CH, absorption of toxic elements by plants,…) → **Elemental maps**

Quantitative:

Concentration of the elements in the sample

Crucial in environment applications (concentration of toxic elements in soil, food, APM,…)
Can be tricky because of matrix effects. The sample must be prepared to make it homogeneous

❑ Features of XRF

- **Qualitative**
- **Quantitative**
- **Multi-elemental**

  In most cases the information about different elements is obtained with just one spectrum
- **Fast**

  If the interest is about major/minor elements. For trace elements measuring time can be quite long
- **Non-invasive**

  No need to perform a sampling
- **Non-destructive**

  Almost every material is not damaged by irradiation with X-rays
- **Portable**

  Thanks to miniaturization of components that can be powered by batteries. Only feature not available at synchrotron!

❑ Conventional XRF

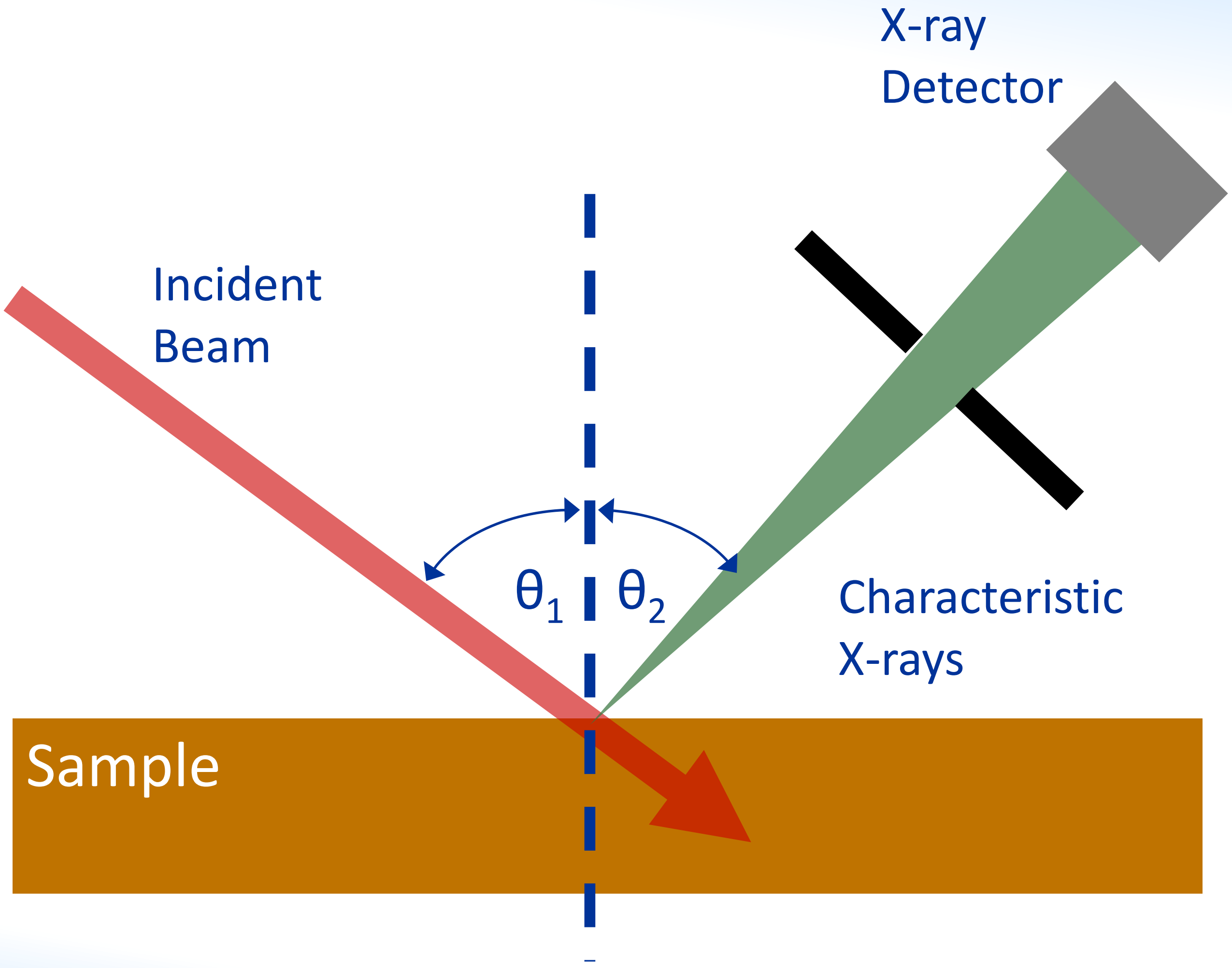

❑ X-ray optics

Refractive index: $\boldsymbol{n = \frac{c}{u_p}}$

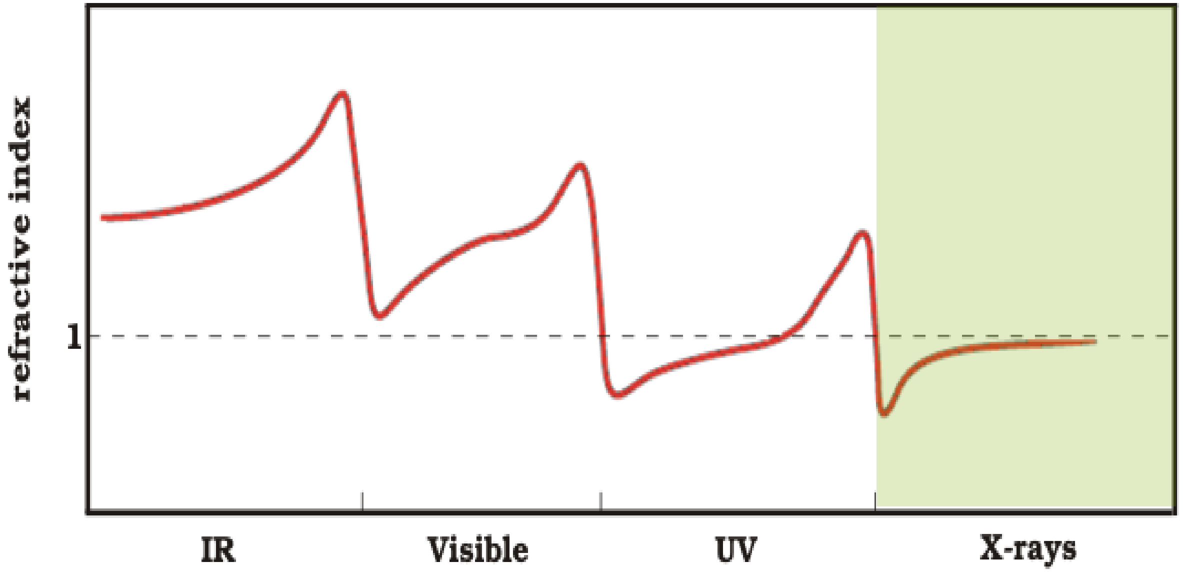

$$n = 1 - \delta + i\beta$$

β = Attenuation term
δ = Phase term

❑ X-ray total reflection

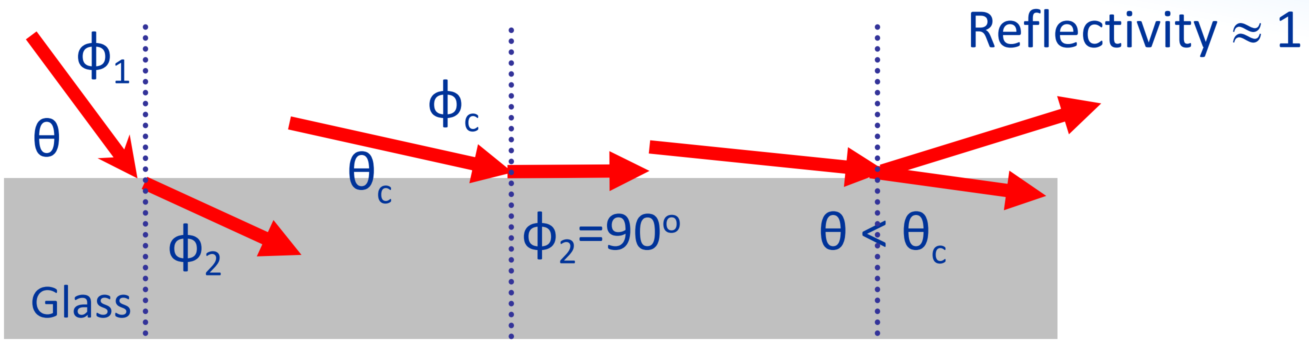

Snell Law $\frac{\sin\phi_2}{\sin\phi_1} = \frac{1}{n} \Rightarrow \sin\phi_2 = \frac{\sin\phi_1}{n} \Rightarrow \phi_2 > \phi_1$ $\qquad n \approx 1 - \delta$

$\vartheta_{crit} = \sqrt{2\delta}$ $\qquad \vartheta_{crit}(deg) \approx \frac{1.651}{E(keV)}\sqrt{\frac{Z}{A}\rho(\frac{g}{cm^3})}$

Z: Atomic number
A: Atomic mass
ρ: Density

❑ X-ray Standing Wave

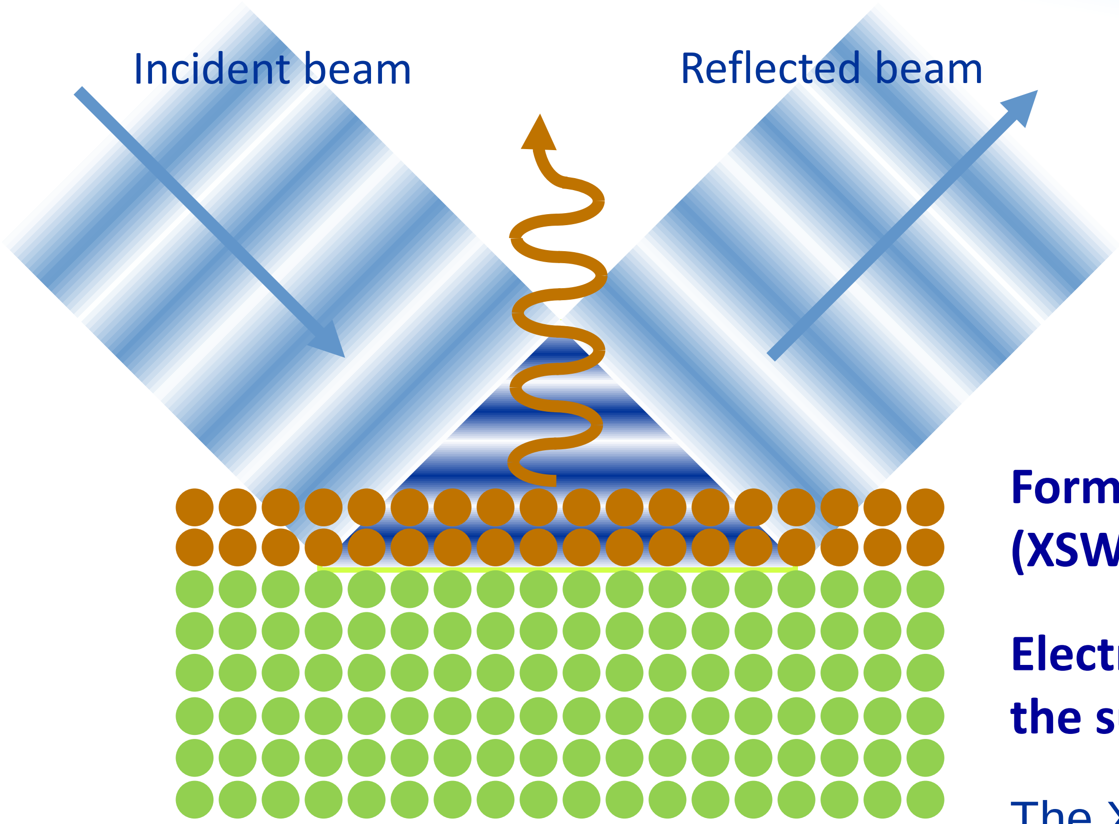

Formation of X-ray Standing Wave (XSW) at grazing incident/exit angle

Electric Field Modulations above the surface

The X-ray fluorescence intensity from the sample depends on the varying field intensity of the XSW field within the sample

GIXRF and XRR

By varying continuously the grazing incident angle through and few times above the critical angle for TR, the recorded XRF intensity profiles (Grazing Incidence-XRF analysis) have the potential to provide information on structural and compositional properties of thin films, such as the layer composition, sequence, thicknesses and densities, interface roughness, in depth elemental gradients of matrix elements or dopants in semiconductors, characterization of nano-particles deposited on flat surfaces, etc

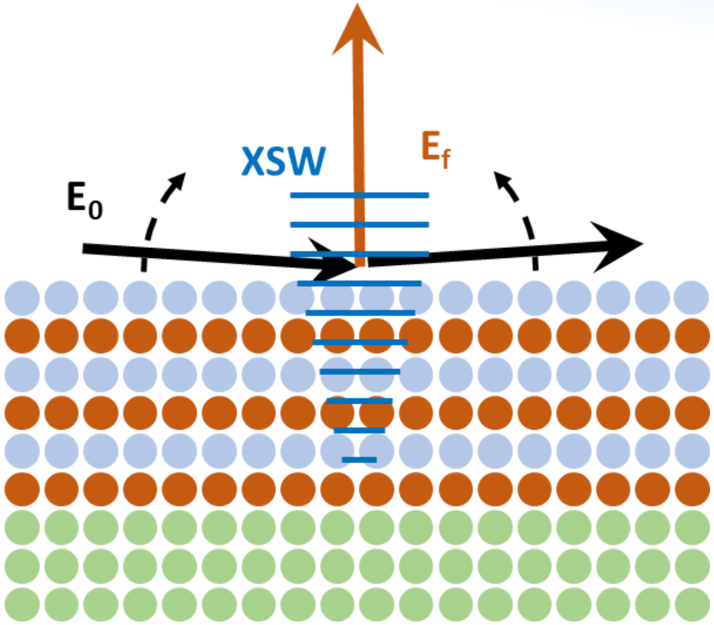

A more accurate and robust reconstruction of these thin film properties requires the synergy or even the simultaneous fitting of GI-XRF with X-ray reflectometry (XRR) data

❑ Total reflection X-ray Fluorescence

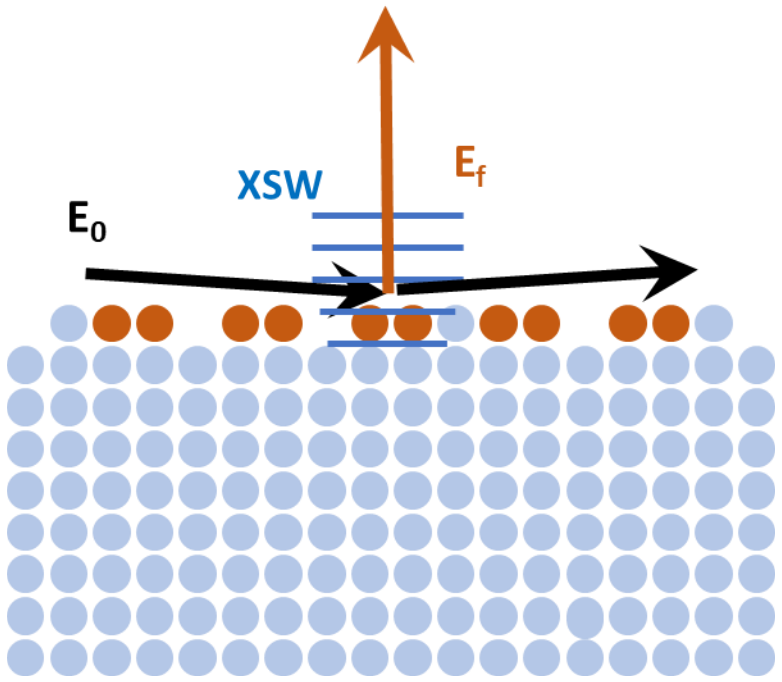

TXRF is essentially an energy dispersive XRF technique arranged in a special geometry.

Due to this configuration, the measured spectral background in TXRF is less than in conventional XRF. This reduction results in increased signal to noise ratio.

TXRF is a surface elemental analysis technique often used for the ultra-trace analysis of particles, residues, and impurities on smooth surfaces.

The joint IAEA-Elettra XRF beamline at Elettra Sincrotrone Trieste

Elettra Sincrotrone Trieste

IAEA
International Atomic Energy Agency
Atoms for Peace

❑ Optical layout

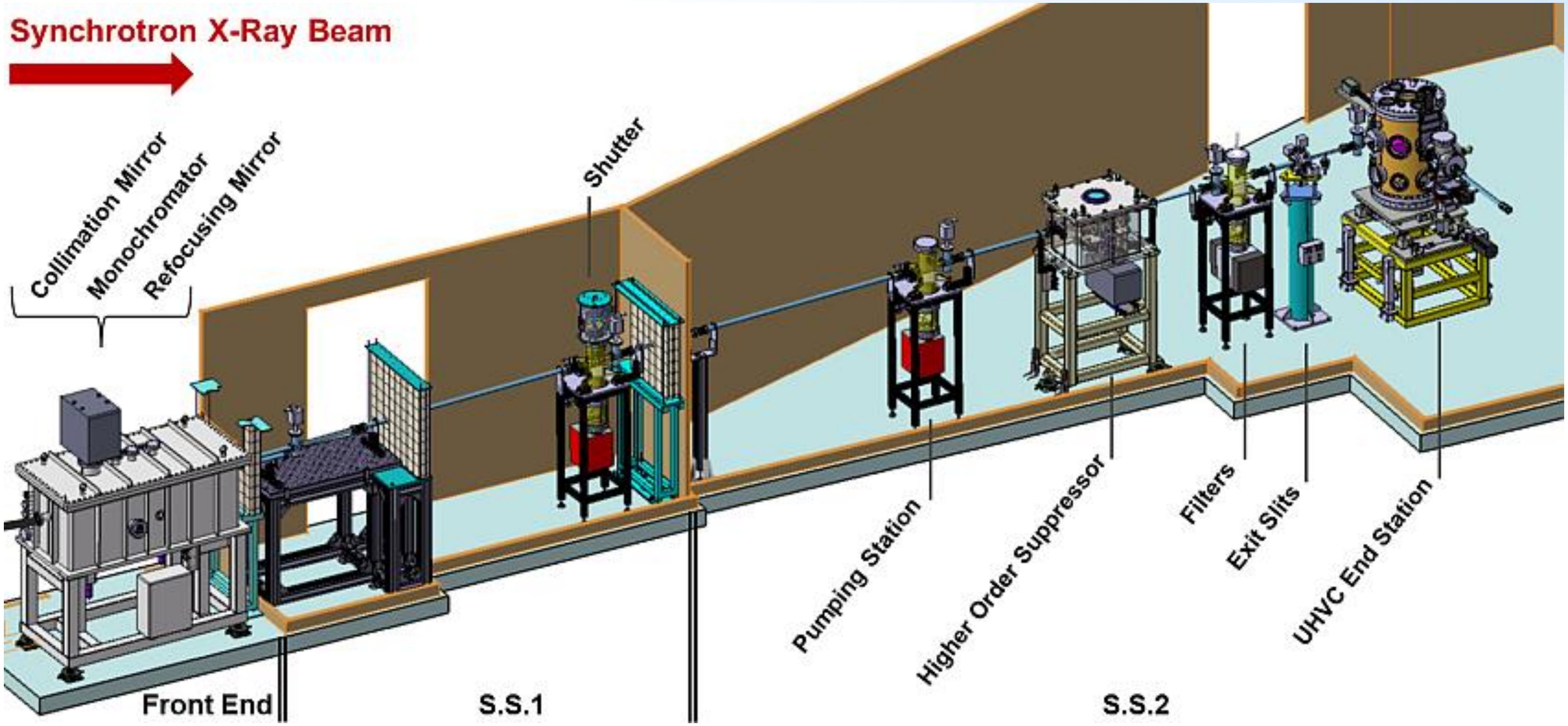

Source	**Bending magnet**
Flux	10^{10}ph/s (at 5 keV for 2.0 GeV, at 10 keV for 2.4 GeV) (Si 111)
Spot size	**250 x 100 (H x V) µm²**
Beam divergence	< 0.15 mrad (at exit slits)

Werner Jark, Diane Eichert, Lars Luehl, Alessandro Gambitta, *Optimisation of a compact optical system for the beam transport at the x-ray fluorescence beamline at Elettra for experiments with small spots*, Proc. SPIE 9207, Advances in X-Ray/EUV Optics and Components IX, 92070G, 2014; doi: 10.1117/12.2063009

❑ The monochromator at XRF

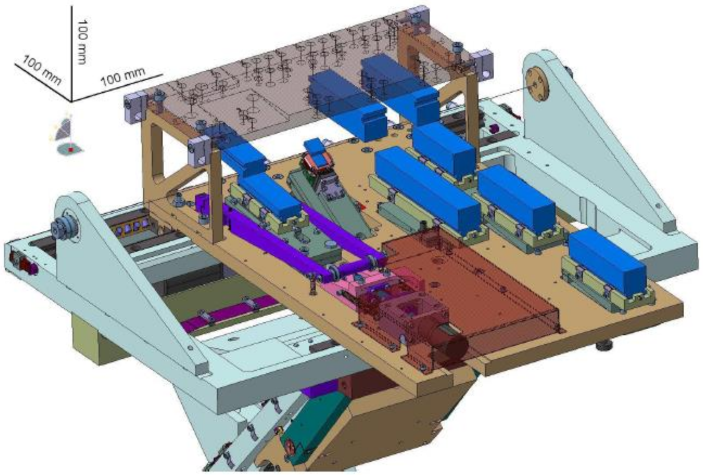

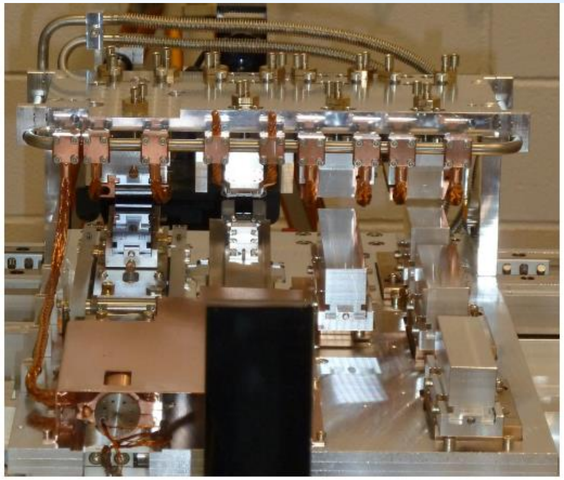

Optics type	E range (keV)	E resolution (ΔE)
Si(111)	3.6 - 14	~ 1 eV at 7 keV
InSb(111)	2.0 – 3.8	~ 1eV at 2.2 keV
ML: High E (RuB_4C)	4.0 – 14.0	~ 55 eV at 1 keV ~ 180 eV at 14 keV
ML: Medium E (NiC)	1.5 – 8.0	
ML: Low E (RuB_4C)	0.7 – 1.8	

Werner Jark *et al.*, Proc. SPIE 9207, Advances in X-Ray/EUV Optics and Components IX, 92070G, 2014; doi: 10.1117/12.2063009

❑ IAEAXspe endstation

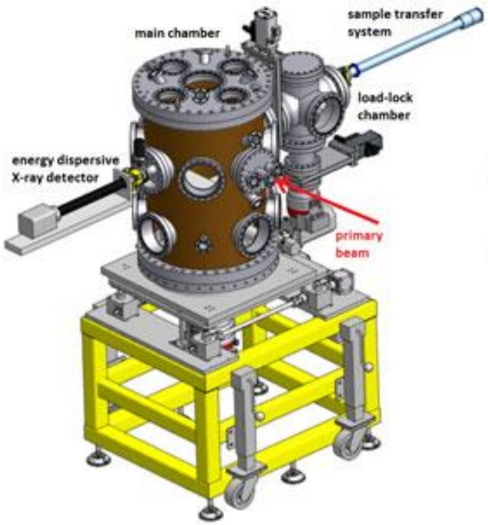

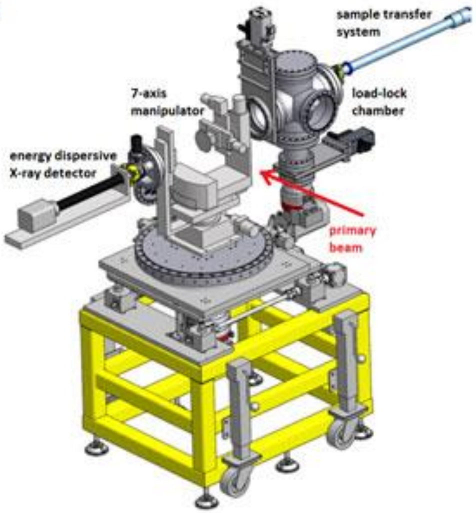

The IAEA end-station is based on a prototype design by Physikalisch - Technische Bundesanstalt (PTB, Berlin) and Technical University of Berlin (TUB)

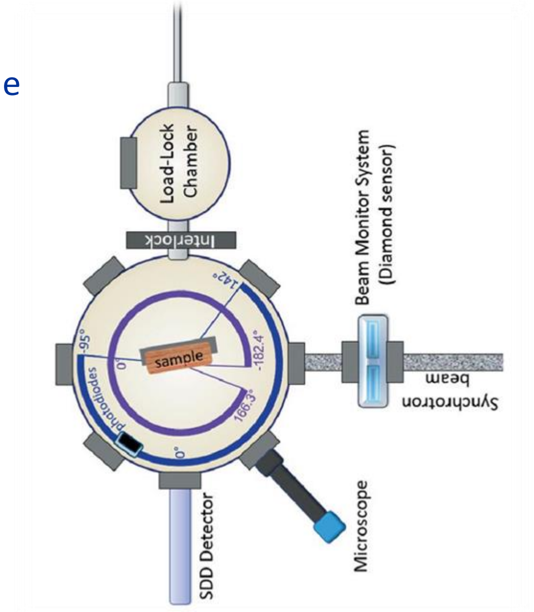

Available detectors:

- Diamond detector for I_0
- SDD detector for **XRF** (different variants) and **XAS** (in fluorescence geometry)
- Photodiodes for **XAS** in transmission geometry
- Photodiodes with 100 and 200µm slits and SDD for **XRR**

Andreas G. Karydas et al., J. Synchrotron Rad. (2018). **25**, 189–203

❑ 7-Axis Manipulator

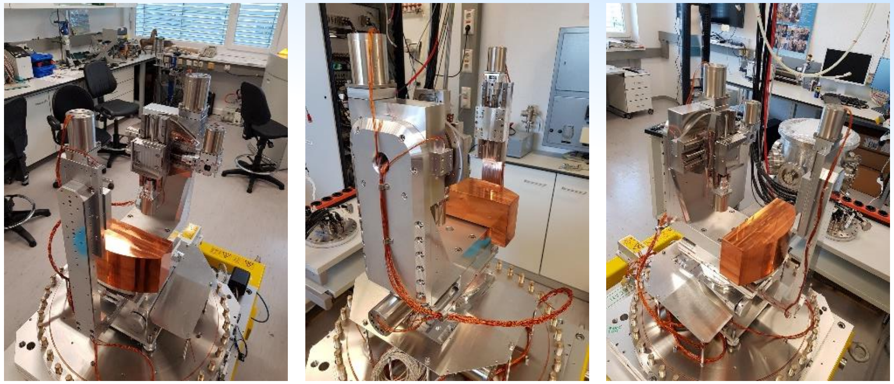

Sample arm

- 3 linear stages (X, Y, Z)
- 2 goniometers (Theta, Phi)

Photodiodes arm:

- 1 linear stages (diode)
- 1 goniometer (2Theta)

- Sample can be moved in various directions/ orientations with respect to the exciting X-ray beam or with respect to the detectors.

- Ultra Thin Window (UTW) Bruker Silicon Drift detector (30 mm^2, FWHM 131 eV @ Mn-Ka), Si photodiodes

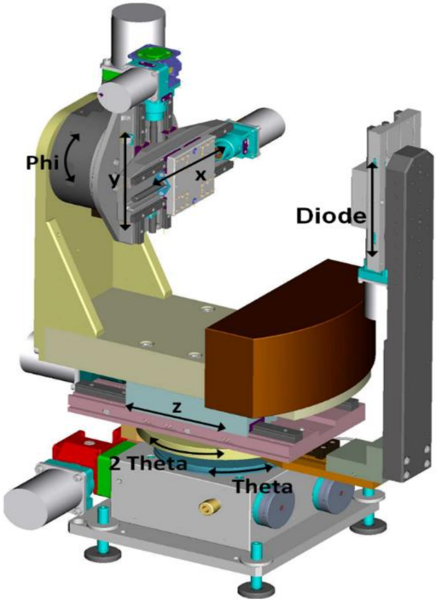

Full step resolution
Linear axes: Diode, X, Y, Z (0.005mm, 0.005mm, 0.0005mm, 0.01mm)
Goniometers: Theta, 2theta, phi (0.001°, 0.001°, 0.005°)

IAEA Coordinated Research Project

- **Materials Science**: Structured materials for energy storage and conversion technologies
- **Nanomedicine - Biosensing technologies**
- **Environmental monitoring** (air particulate matter, water)
- **Biological:** Elemental distribution/ speciation on plant organ (leaves, roots, shoots, seeds, etc.)
- **Cultural Heritage –preventive conservation**
- **Food products security – Authenticity**
- **Determination of X-Ray Fundamental Parameters**

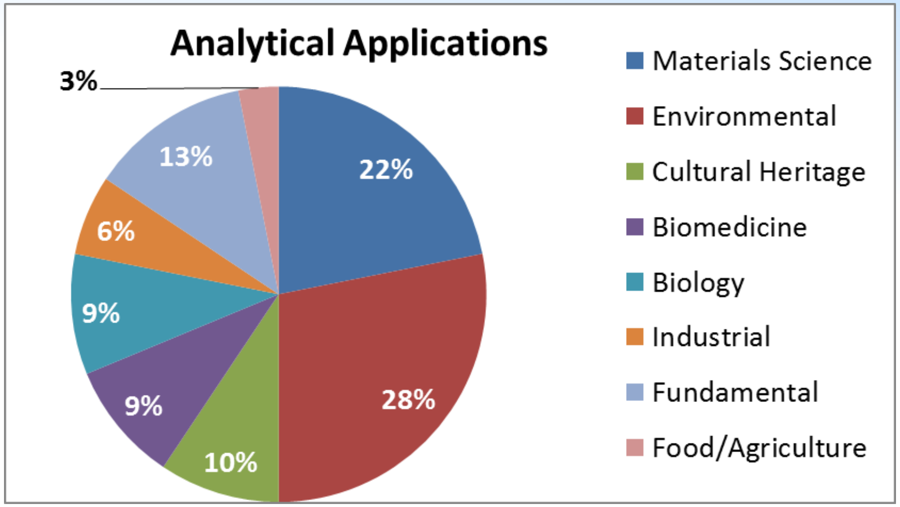

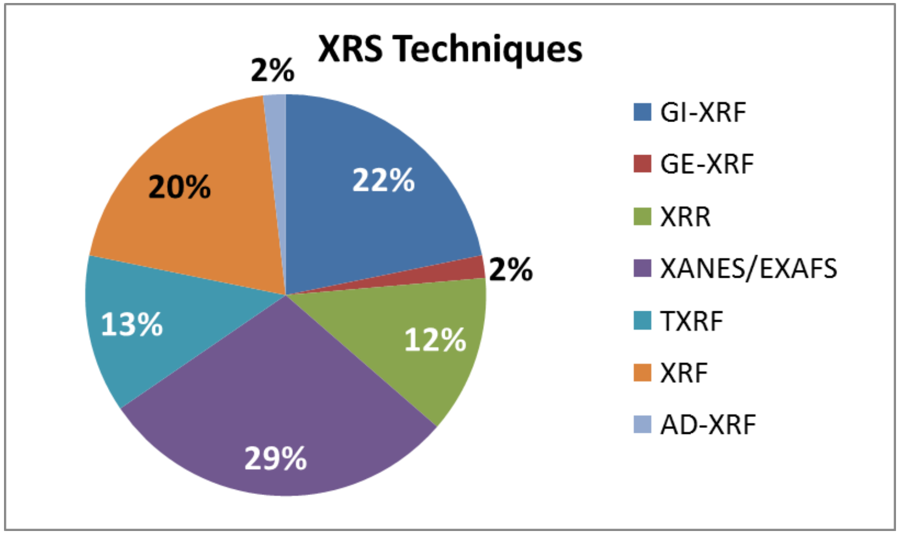

❑ non-UHV compatible samples

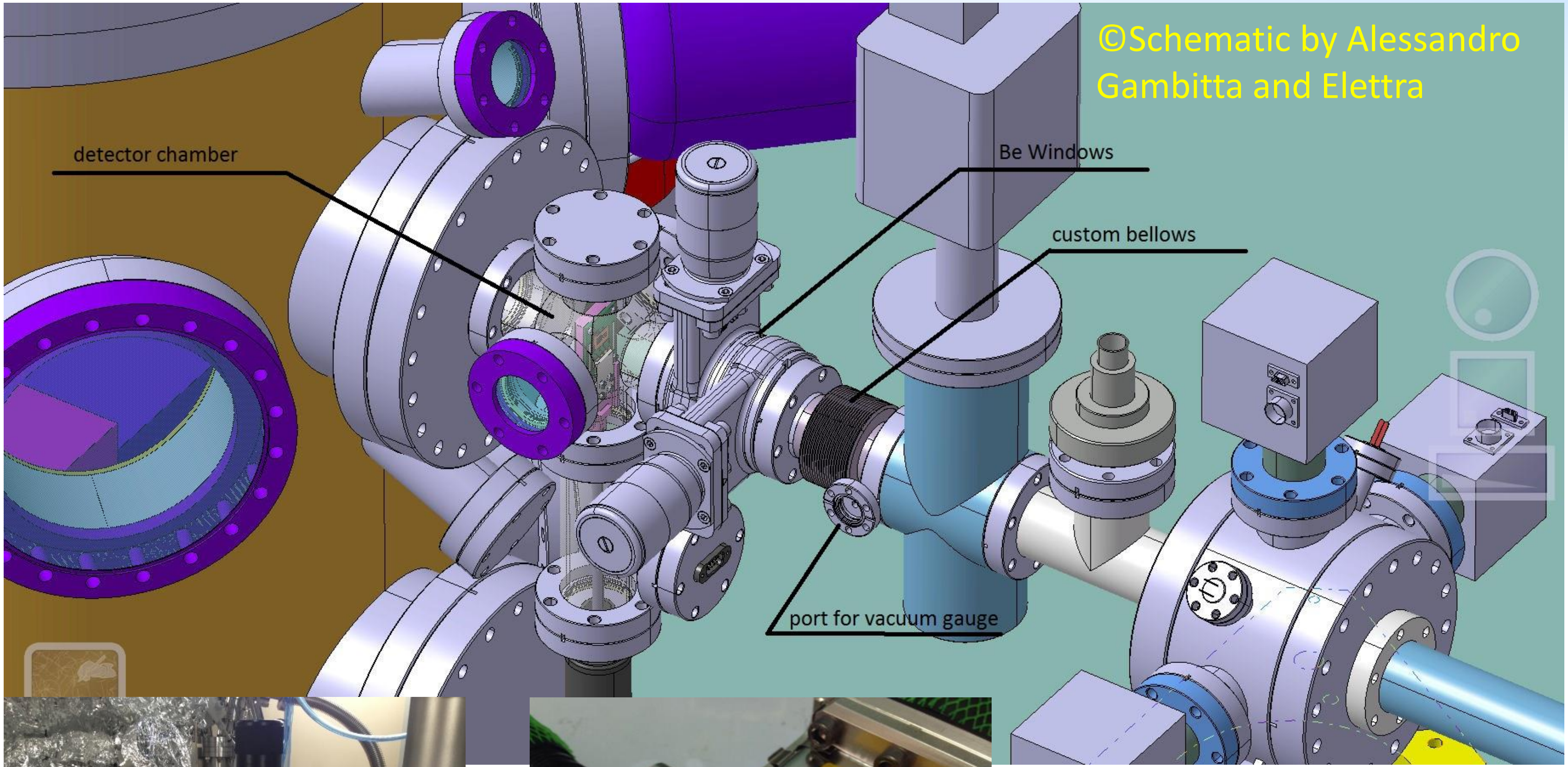

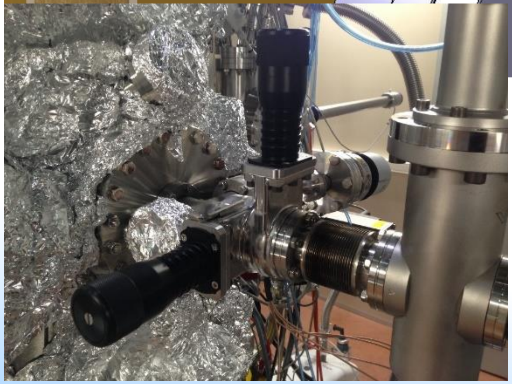

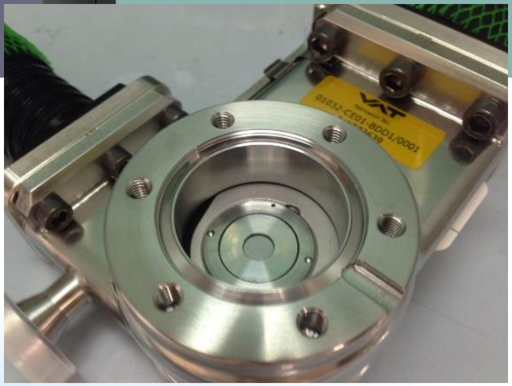

20µm IF-1 Beryllium
Luxel Corporation

Geometries and techniques

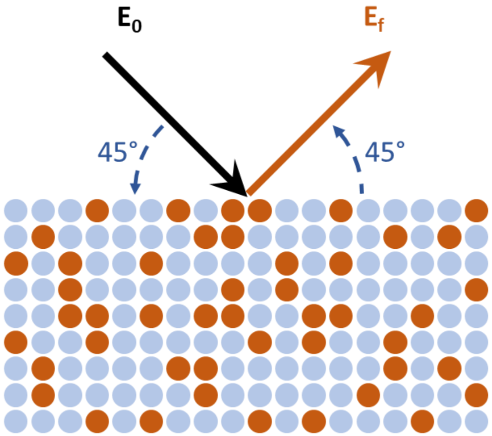

Standard 45°/45° - XRF

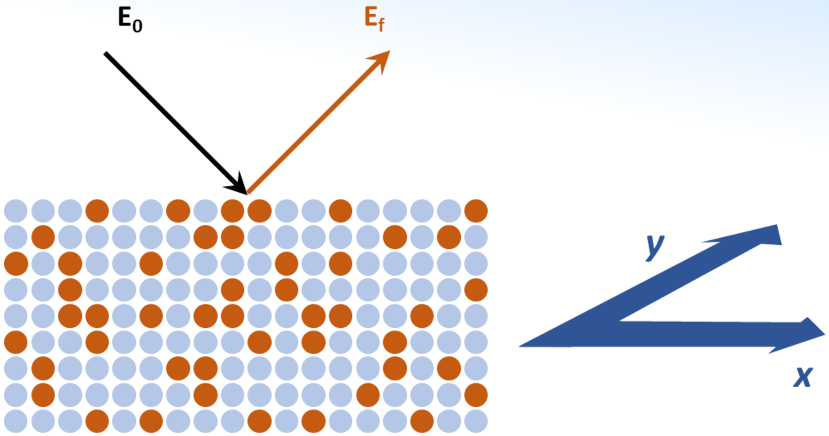

micro - XRF

Elemental characterization

Mapping

X-ray Absorption Spectroscopy
(on hot spots)

Grazing angle geometries

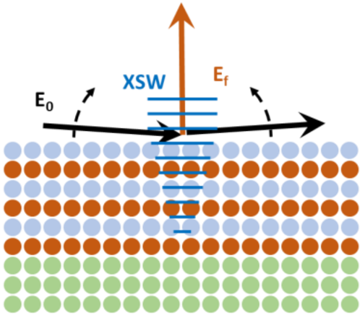

Grazing Incident - XRF

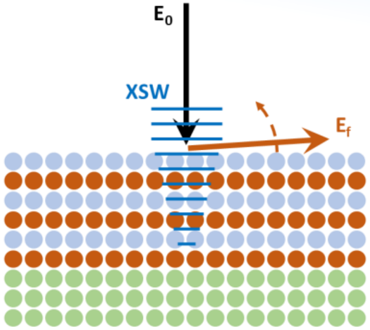

Grazing Emission - XRF

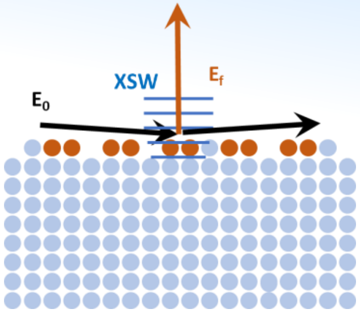

Total reflection - XRF

Depth profiling
measurements

Trace element analysis
Surface contamination

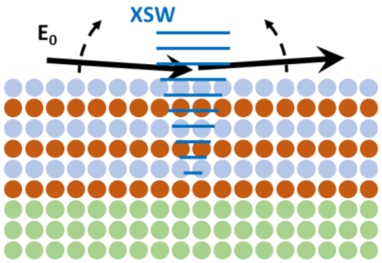

X-Ray Reflectometry

X-ray Absorption Spectroscopy
(in TXRF geometry)

Detector geometry for TXRF

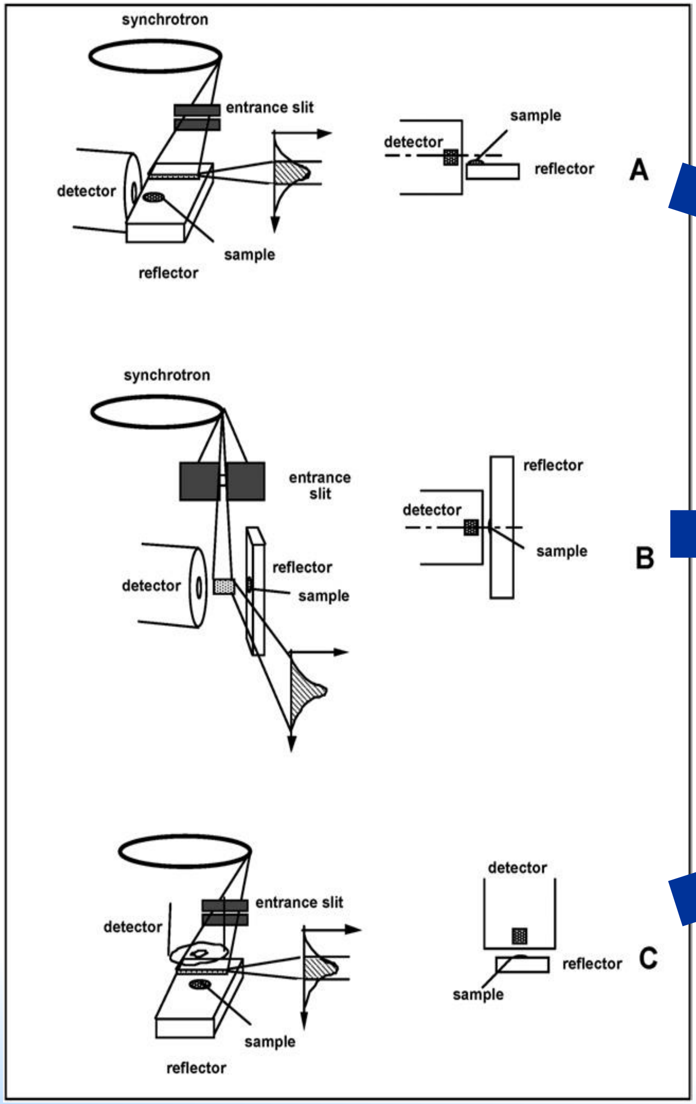

The beam is naturally vertically collimated (0.1-0.2 mrad) and has linear polarization in the orbit plane

Good excitation
No scattering
Poor detection

Poor excitation
No scattering
Good detection

Good excitation
Scattering
Good detection

C. Streli, P. Wobrauschek, F. Meirer and G. Pepponi, *Synchrotron radiation induced TXRF*, J. Anal. At. Spectrom., 2008, 23, 792–798, DOI: 10.1039/b719508g

❑ GIXRF: C/Ti double layer

Prepared and characterized by AXO Dresden

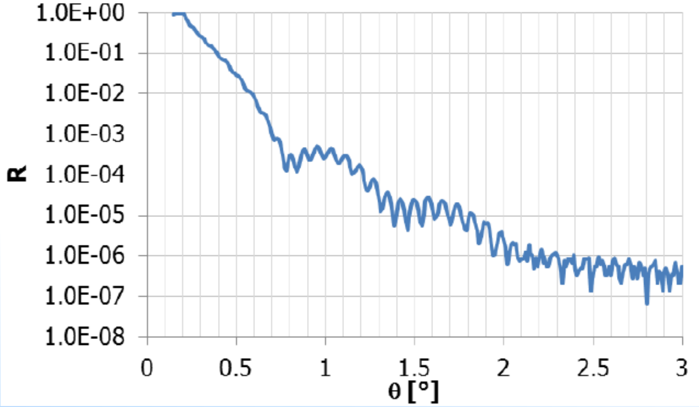

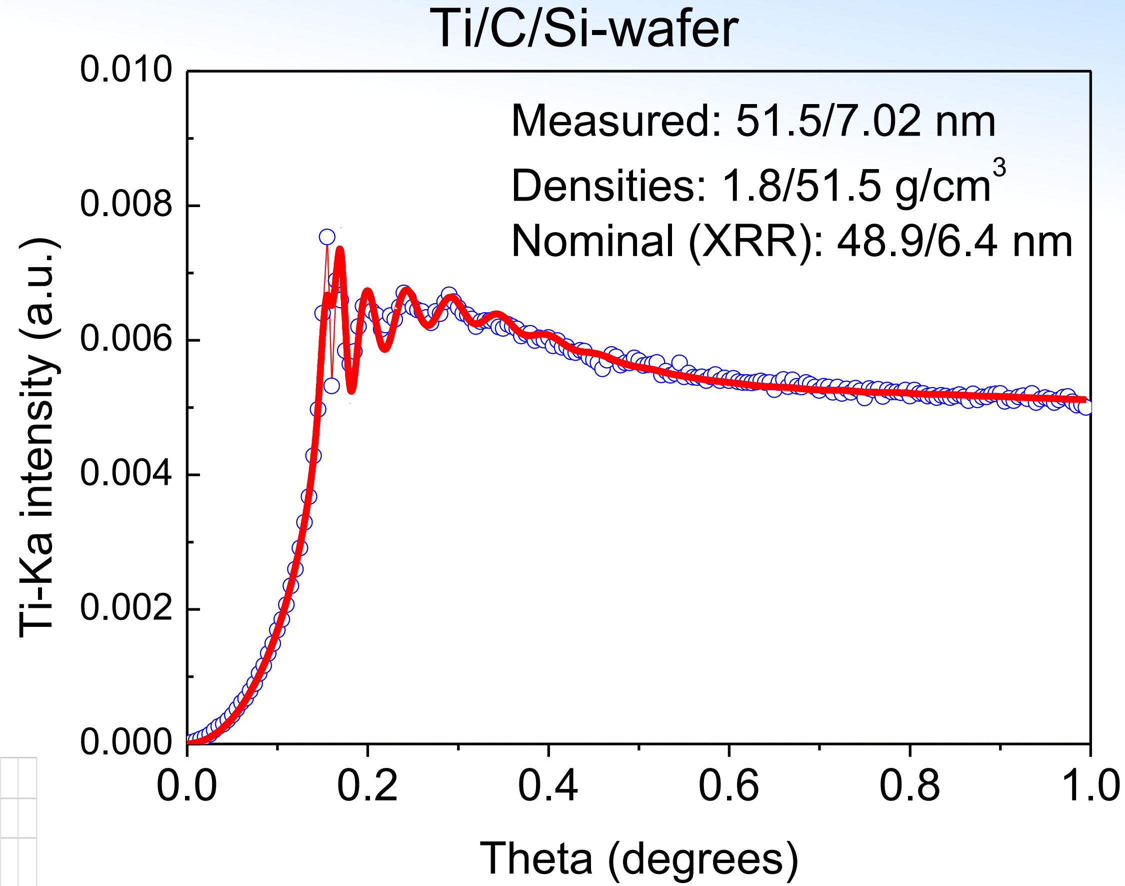

	Fit	**Nominal**
Ti (nm)	7.0	6.4
C (nm)	51.5	48.9

❑ W/B$_4$C multilayered (x15) thin film

Multilayered sample, prepared by the Ramanna Center for Advanced Technology, Indore, India

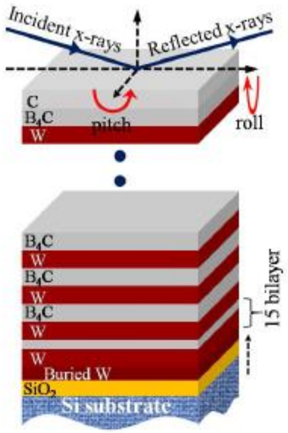

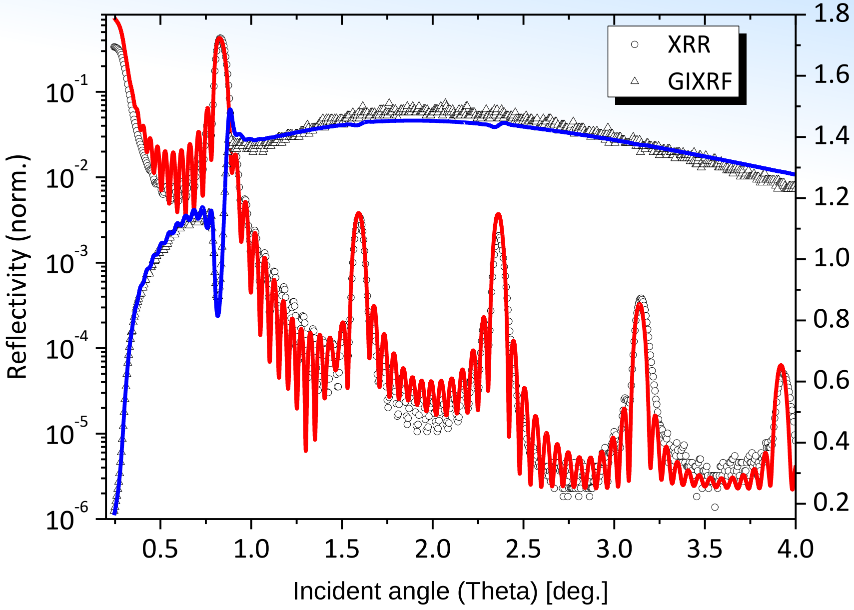

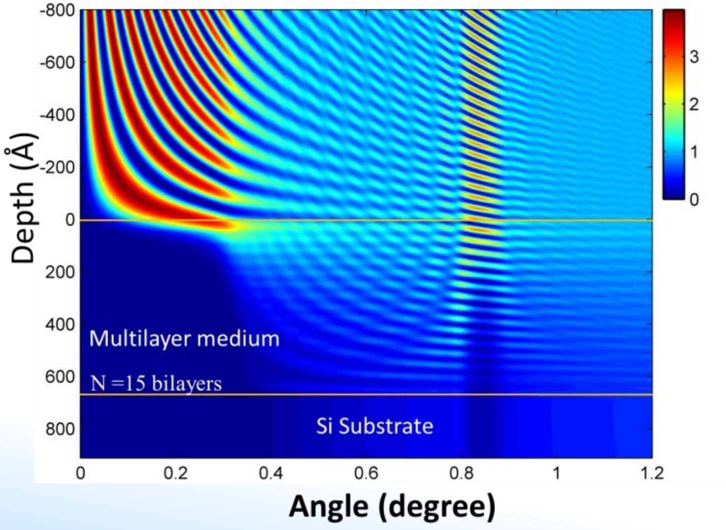

Electric Field Intensity (Normalized)

		'B$_4$C'/'W' multilayer		
Layer Material	Periodicity	Thickness (nm)	Roughness (nm)	Density (g/cm^3)
B$_4$C	14	1.9 ± 0.1	0.2 ± 0.1	2.10 ± 0.2
W		2.4 ± 0.2	0.3 ± 0.1	16.0 ± 0.2
B$_4$C	1	2.1 ± 0.6	0.45 ± 0.2	2.3 ± 0.2
W		3.6 ± 0.3	0.55 ± 0.2	15.5 ± 1.0
SiO$_2$	1	2.0 ± 0.3	0.5 ± 0.2	2.0 ± 0.3

good agreement with previous analyses performed at the BL-16 beamline of Indus II

Zn speciation in fractionated APM

9-stage May-type cascade impactor

Sampling of size fractionated aerosol, down to 0.07um size

20-3200 L of air

Deposited particles form a stripe of 200-500 µm width on the 20x20 mm^2 Si wafer

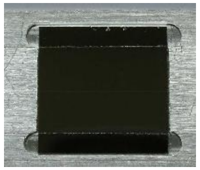

Sample geometry well suited to SR-TXRF-XANES investigations!

J. Osan, Environmental Physics Department, Centre for Energy Research, Budapest, Hungary

*Self-absorption correction as described in: Osán J et *al.*, Spectrochim Acta Part B 65 (2010) 1008-1013

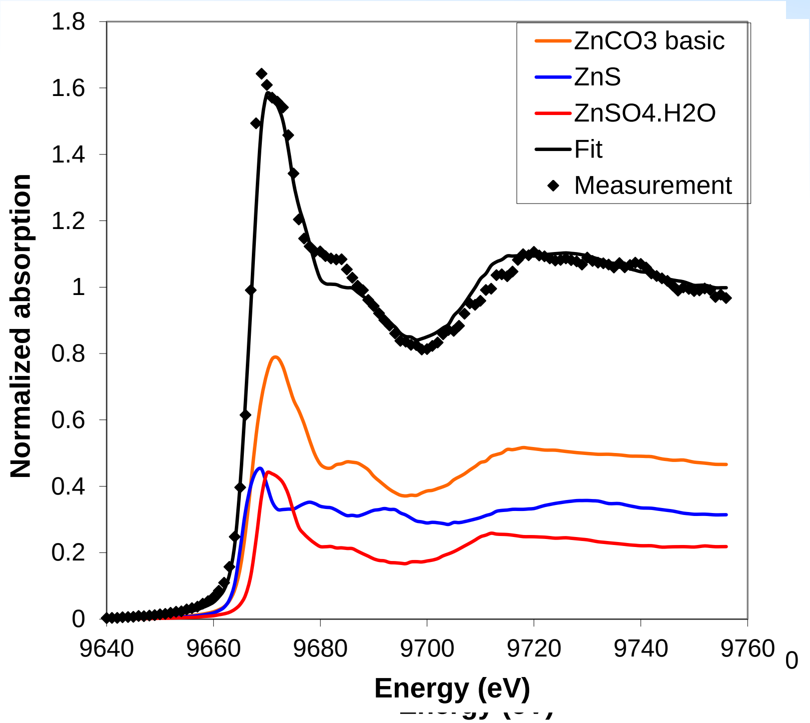

Sample: Budapest (Hungary), 0.15–0.3 µm, Zn content: 239 ng/m3 (84 ng on 20 mm strip)

47% $ZnCO_3$, 32% ZnS, 22% Zn in glass*

Main source: **Burning of painted wood**

Sample: Paks (Hungary), 0.3–0.6 µm, Zn content: 71 ng/m3 (28.5 ng on 20 mm strip)

38% $ZnSO_4$, 40% ZnS, 22% Zn in glass*

Main source: **Iron smelter**

❑ Aerosols from 3D metal printing

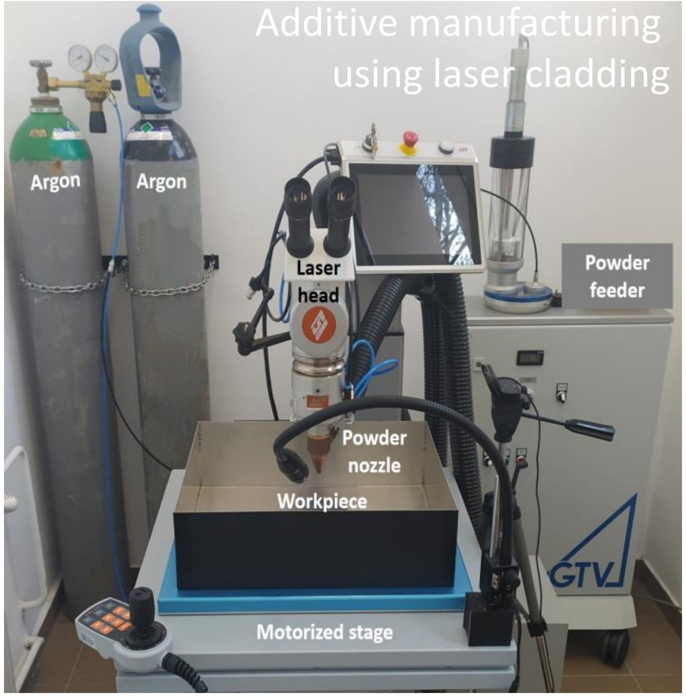

Figure courtesy: Attila Nagy, Wigner FK, Budapest, Hungary

XANES: Elettra XRF and XAFS beamlines

Cr oxidized – oxidation number ~+1.0
No significant amount of Cr^{6+} detected

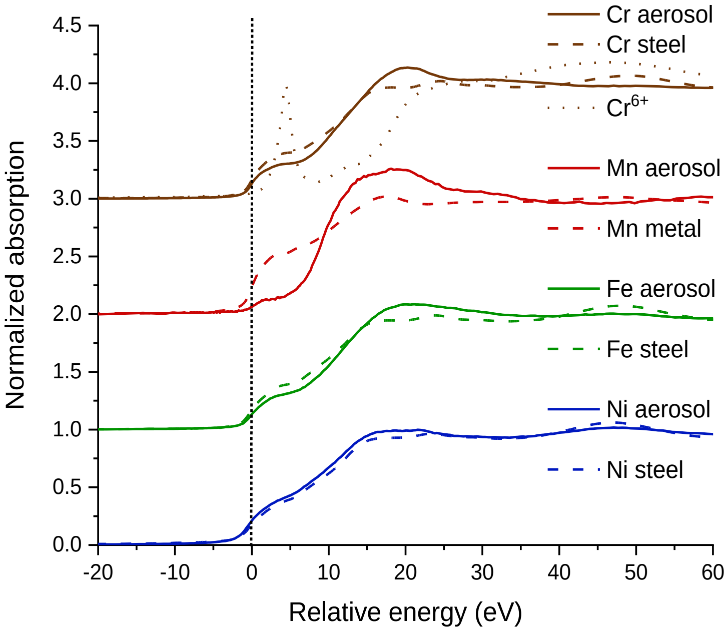

Mn mostly oxidized – oxidation number ~+2.3

Fe slightly oxidized – oxidation number ~+0.7

Ni mostly metallic – oxidation number ~+0.1

Most of emitted aerosol particles are in the ultrafine range

Oxidation number increases with decreasing particle diameter – important for estimation of health effects

S. Kugler et al., Spectrochim. Acta Part B 2021, 177, 106110

Se and Hg in edible mushrooms

K. Vogel-Mikuš [1], P. Kump[2], I. Arčon[3]
[1] Biotechnical faculty, University of Ljubljana, [2]Jozef Stefan Institute,
[3] University of Nova Gorica

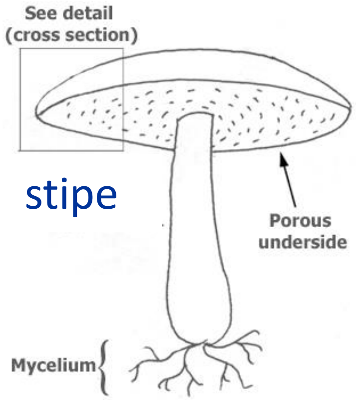

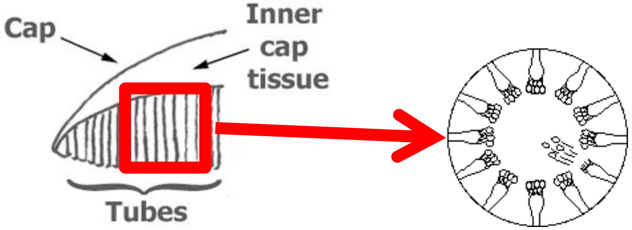

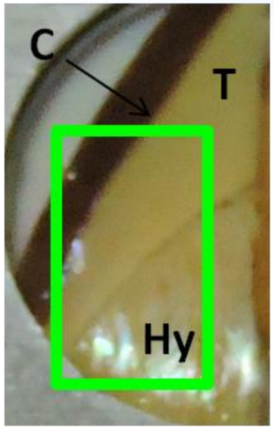

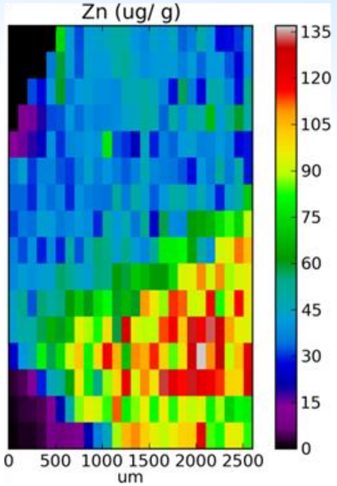

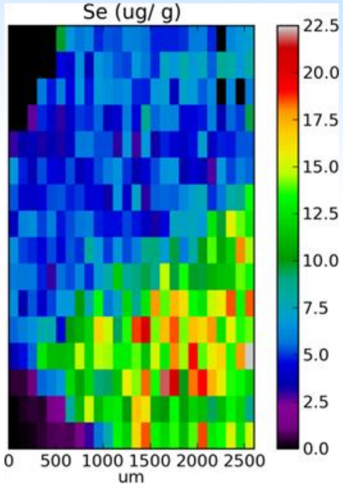

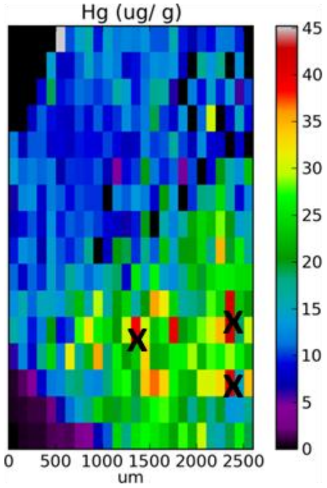

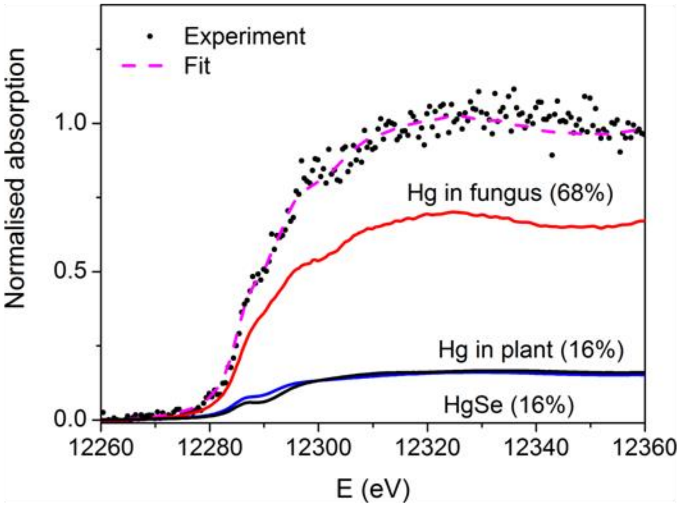

Hg is bound to tetra-cysteine proteins (metallothioneins). These proteins are digested by enzyms in the stomach and Hg is released and absorbed in our body.

☐ GI-XANES on Black Glaze

Fe-based decorations of Ancient ceramics manufactured in South Italy

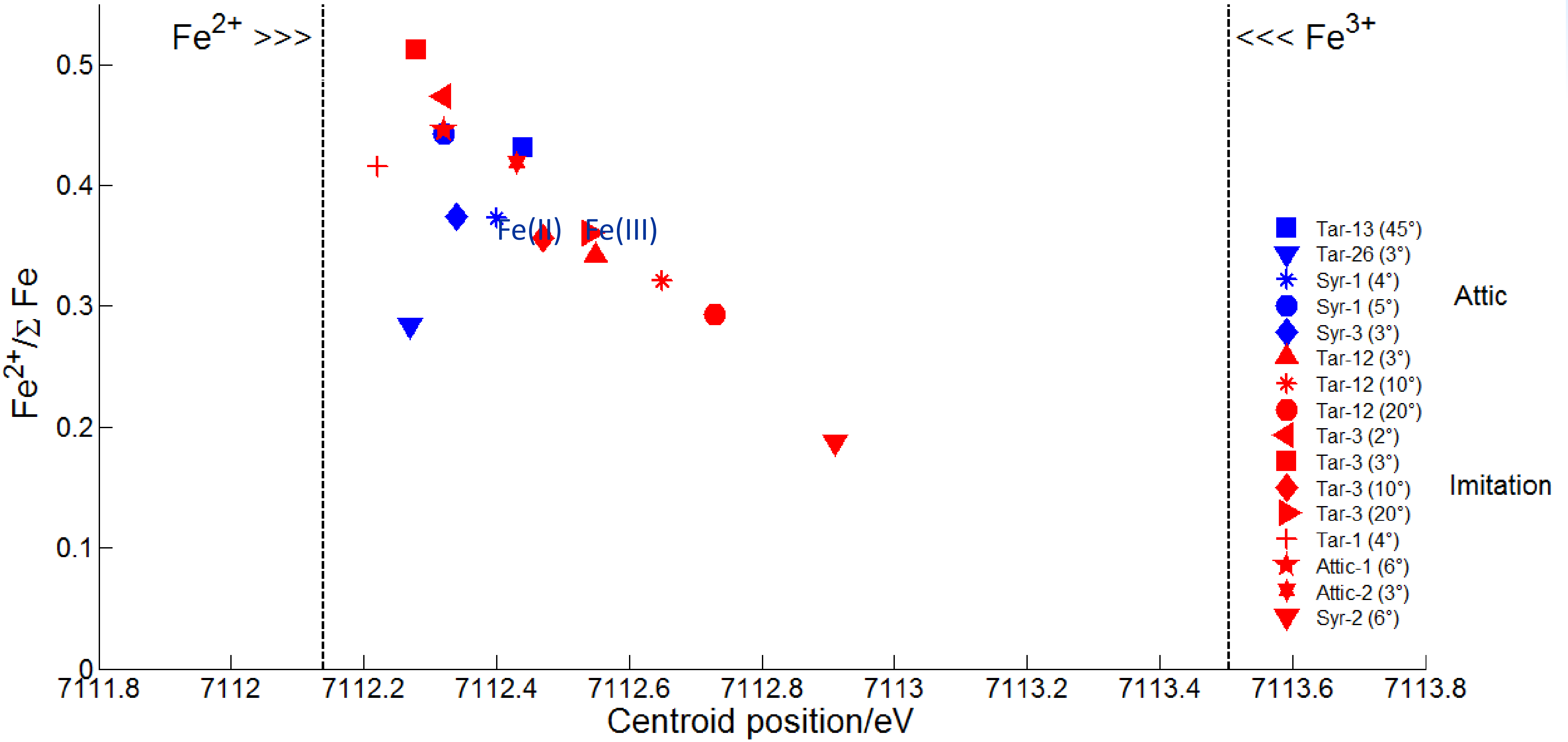

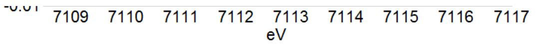

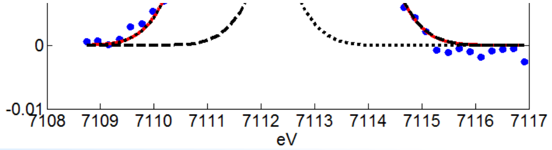

Taranto Archeological Museum Apulo f.r. Anonymous (Half IV cent. b.C.)

P. Romano, C. Caliri
INFN-LNS, Catania, Italy

❑ Analysis of gold samples

Absorption edges of Pt and Au

	Pt	Au
Z	78	79
L1 (keV)	13.88	14.353
L2 (keV)	13.273	13.734
L3 (keV)	11.564	11.919

Pt La: 9.44 keV

Incident energies employed: 11600, 11650, 11700, 11800 eV

Synchrotron XRF spectra of pure (99.99%) thick (thickness 25 μm) gold samples

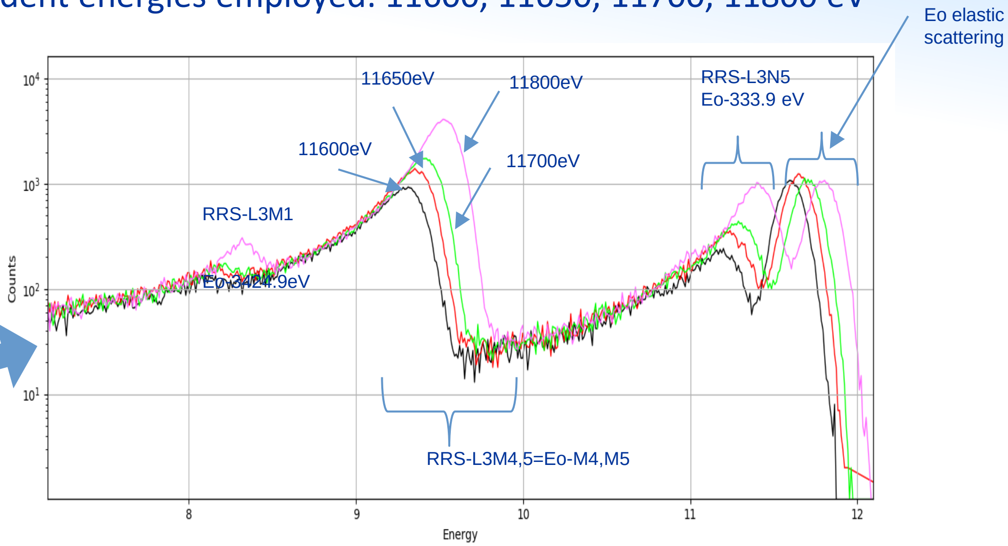

Eo=11600 eV @Elettra

Pure gold spectrum vs. Gold alloy with 0.15% Pt (Au:65.56%, Cu:25.21%, Ag:9.08%) and vs. a different certified alloy of similar composition without Pt

11600 eV > Pt(U_L3)=11564 eV

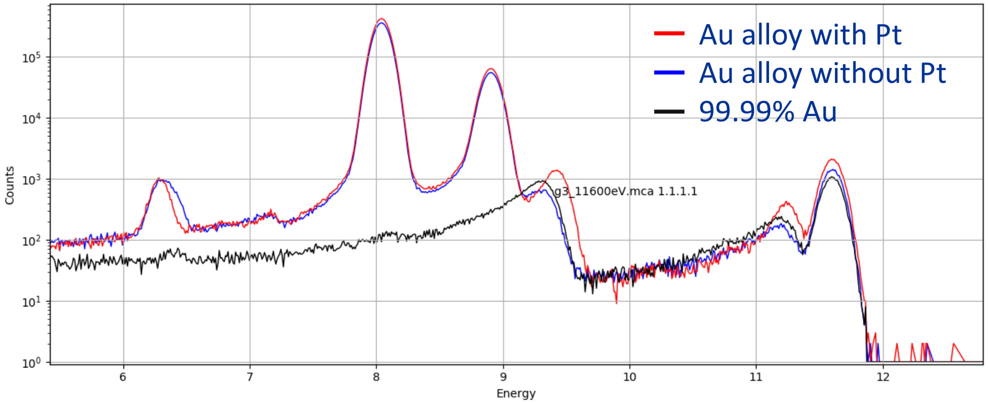

Courtesy of A.G.Karydas, (National Center for Scientific Research "Demokritos", Greece)

IAEA
International Atomic Energy Agency

Thanks for your attention!

Alessandro Migliori

a.migliori@iaea.org

https://nucleus-new.iaea.org/sites/nuclear-instrumentation/Pages/Home.aspx

https://www.elettra.trieste.it/lightsources/elettra/elettra-beamlines/microfluorescence/x-ray-fluorescence.html